J. Indian Inst. Sci.
A Multidisciplinary Reviews Journal
ISSN: 0970-4140 Coden-JIISAD

REVIEW ARTICLE

C–H···Y (Y=N, O, π) Hydrogen Bond: A Unique Unconventional Hydrogen Bond

Sanat Ghosh[1,2] *and Sanjay Wategaonkar*[1*]

Abstract | We present a spectroscopic overview of the C–H···Y (Y = hydrogen bond acceptors) hydrogen bonded (HB or H-bond) complexes in this article. Although C–H···Y interactions have been recognized as H-bonding interactions for quite some time, they have not been investigated spectroscopically until recently. Recent results indicated that unlike the conventional hydrogen bond, C–H···Y H-bond has interesting spectroscopic characteristics, i.e. it shows both red as well as blue shift in C–H stretching frequency upon H-bond formation. This review presents examples of red, blue, and zero shifted C–H···Y H-bonds investigated in our laboratory that were characterized using laser-based IR and UV spectroscopic techniques applied to the cold isolated molecular complexes formed under supersonic expansion conditions. Along with spectroscopic information, ab initio/DFT-predicted geometry optimized structures of various conformers, harmonic frequency calculations of the optimized structures, and a number of properties such as electron densities at the bond critical points, orbital interaction energies, binding energies of the C–H···Y bound complexes are also summarized for better understanding of this type of H-bond. Not only the spectroscopic shift in C–H stretching frequency, but also the role of C–H···O H-bonds in microsolvation of several organic molecules has been highlighted. It has been found that depending upon activation of C–H moiety, C–H···Y H-bonds can provide primary or secondary stabilization for the growth of the primary solvation shell around organic molecules.

1 Introduction

Intermolecular interactions are known to play a very important role in governing physical and chemical properties of the matter. In this respect, hydrogen bond (HB or H-bond) is considered as the most important intermolecular interaction, spanning its abundance and functions in small molecules like water to biological macromolecules as well as inorganic and organic supramolecules. The concept of H-bonding interaction is centuries old and dates back to 1912 when Moore and Winmill first described a weak union in trimethylammonium hydroxide to explain its weaker basic properties compared to tetramethylammonium hydroxide[1,2]. In 1920, Latimer and Rodebush suggested that the interaction in binary complexes such as (H_2O–H_2O or H_2O–NH_3) is due to the fact that 'the hydrogen nucleus held between two octets constitutes a weak 'bond'[3]. However, none of them referred these weak interactions as H-bonding interactions. Linus Pauling for the first time described such interactions as H-bonding interactions in his famous book 'The Nature of the Chemical Bond'. Soon after that, a lot of work was carried out to understand the role and nature of these interactions. Extensive studies on this interaction concluded that this interaction is ubiquitous in chemistry and biology and plays a decisive role in providing a three-dimensional structure of large bio-polymers like protein,

[1] *Department of Chemical Sciences, Tata Institute of Fundamental Research, Homi Bhabha Road, Mumbai 400 005, India.*
[2] *Present Address: Universidad Complutense de Madrid, Madrid, Spain.*
**sanwat@tifr.res.in*

DNA, other organic and inorganic supramolecular species. Many physical and chemical processes like solvation, proton transfer, crystal growth, enzymatic reactions, and molecular recognition are all greatly controlled by this interaction.

Hydrogen bond can be depicted as X–H···Y, where the three dots indicate H-bond. In most of the cases, X and Y are strongly electronegative atoms such as O, N, and halogens and the interaction is termed as a conventional H-bond. Apart from the conventional hydrogen bond, currently a variety of unconventional H-bonds have been identified[1,4–6]. In this respect, C–H···Y H-bond has got quite a bit of attention recently, because of its significant contribution in chemistry and biology. Like the conventional H-bond, the C–H···Y H-bond is also a very old concept. Kumlar in 1935 explained that HCN is liquid due to the weak association of the HCN molecules via C–H···N interactions[1]. Subsequently, Glasstone in 1937 and Pauling in 1939 mentioned the existence of the C–H···Y interaction to explain the abnormal physical properties of some of the liquids[1]. A systematic study of C–H···Y H-bonding was reported by Sutor[7,8] in 1962, where she analysed the X-ray crystal structures of several purine and pyrimidine bases and found frequent short contact distances (shorter than the corresponding van der Waals distances) between C atom of C–H moiety and O atom of the neighbouring molecules. Sutor's work was strongly criticized by other contemporary scientists who had reservations about the accuracy of the distances reported in the crystal structures. This work was followed by Taylor and Kennard in 1982[9] who analysed high-resolution neutron diffraction data of 113 organic crystals and found several such short contact distances in the crystals confirming the existence of the C–H···Y interaction. This study by Taylor and Kennard made a significant impact on the scientific community in believing that the C–H···Y interaction is indeed a real stabilizing interaction. Since then, many researchers have reported the presence of this interaction from the analyses of crystal structures, electronic structure calculations, and spectroscopic studies in gas phase or in cold matrices. The strength of this hydrogen bond was found in general to be lesser than the conventional H-bonds; however, it is strong enough to provide structural rigidity or secondary stabilization in the system. Moreover, as the strengths of these interactions are not high enough, these are easily breakable at RT and that brings about the dynamic behaviour of the systems associated with the C–H···Y H-bonds.

The critical role of C–H···Y HBs in determining the structure of several important biological molecules cannot be underestimated[10–14]. For example, crystal structure analyses of several transmembrane proteins and various DNA structures showed the presence of these interactions. Jiang et al.[15] have calculated stabilization energies of the 469 protein–protein complexes using a statistical potential and found that an average of 17% of the total stabilization of the protein–protein complexes was contributed by the C–H···O H-bonding interactions. Sometimes, this contribution can be as high as 40–50%. Mainly, the α-C–H group of the amino acids, which are activated due to presence of adjacent electron withdrawing groups (>C=O, –NH–), has been found to be participating in the C–H···Y HB interaction. It is also found to be playing an important role in providing 3D structure to many organic and inorganic supramolecular complexes, molecular recognition, and enzymatic catalysis[16–18]. There is a lot of literature[10,15,19–26] available indicating the important role of C–H···Y H-bonds, however, it is beyond the scope of this review.

This review focuses on the spectroscopic studies of C–H···Y H-bond in isolated complexes, which were carried out in our laboratory. It is well known that conventional H-bonds can be characterized using vibrational spectroscopy, where a red shift in the X–H stretching frequency and enhancement of IR transition intensity are used as the indicators of hydrogen bond formation. In the case of conventional hydrogen bonds, the red shift in the X–H stretching frequency is of the order of a few hundred wavenumbers. In this respect, C–H···Y HB is very peculiar as it shows both red shift as well as blue shift in the C–H stretching frequency upon H-bond formation and the shift is of the order of a few tens of wavenumbers[27–46]. The blue shift in the C–H stretching frequency was first reported by Hobza et al. based on the computational study in benzene dimer[47]. Subsequently, a year later, Hobza et al. have experimentally shown that the C–H stretching frequency in fluoroform–benzene and chloroform–benzene complexes get blue shifted by 14 cm^{-1} in both the cases[48]. A blue shift of 7.7 cm^{-1} has been observed in the complex of halomethane with benzene in the gas phase[34]. In all these cases, the C–H moieties form CH···π interaction with the benzene π-cloud. A series of blue shifted H-bonds have been studied in cold matrices by van der Veken et al. For example, dimethyl ether–CHF_3 complex showed a blue shift of 17.7 cm^{-1}[32], and a blue shift as high as 26.7 cm^{-1} was observed in the

fluoroform–acetone complex which has C–H···O interaction[33]. Over the time, many more experimental studies in the gas phase, liquid phase, and cold matrices have shown the existence of the blue shifted H-bond[28,29,43,46,47,49]. For example, fluoroform–fluorobenzene complexes which have either C–H···F or C–H···π interactions showed 12 and 21 cm^{-1} blue shift, respectively[29]. Mikami et al. reported a 2 cm^{-1} blue shift in benzonitrile–$CHCl_3$ complex which has C–H···N interaction[49]. The blue shifted H-bonds were initially termed as 'anti-hydrogen bonds'[47], but later the term was dropped as the term 'anti' evokes destabilization of the system whereas the blue shifted H-bonds provide stabilization to the systems. They were later renamed as 'improper, blue shifting' H-bonds[50]. Various theories have been put forward to explain the blue shifting nature of C–H···Y H-bonds. Among them, the dispersion interactions[47,50], redistribution of electron densities[35,51,52], electrostatic field effect[53,54] and rehybridization[55] have been proposed to explain the blue shifting H-bonds. However, a unified explanation is sparse in the literature. Jemmis et al.[56] have calculated electron densities of several H-bonded complexes and concluded that there was nothing improper in blue shifted H-bond. Red, blue and zero shifts are interplay of the polarity of X–H bond and HB acceptor ability of acceptor.

Combination of IR spectroscopy with supersonic expansion technique is a very powerful technique to obtain the microscopic details of the weakly bound H-bonded complexes. Since supersonic expansion can prepare molecular complexes in their internally cold state and under collision-free conditions, the intrinsic interactions present in the system can be monitored in absence of any perturbation. Moreover, spectral congestion is also greatly reduced and therefore the spectral assignments are much easier. The other advantage is that the experimentally measured quantities for these complexes can be directly compared with the ab initio calculations. Therefore, more insights into these types of H-bonding interactions such as change in electron densities on HB donor and acceptor, HB strength, HB length and other geometrical parameters can be obtained. In the following subsections, a brief overview of the work on C–H···Y HBs that has been carried out in our laboratory is presented. The review is organized in the following order. First the experimental and computational methods will be discussed and then in the subsequent sections, red, blue, and zero shifted H-bonded systems will be presented. In the later sections, the role of C–H···Y H-bonds in microsolvation will be discussed. Figure 1 depicts all the molecules reported in this work.

2 Experimental Methods

All the complexes discussed in the following sections were prepared using supersonic free molecular jet and probed using a variety of UV and IR laser-based spectroscopic techniques. Advantages of using supersonic jet have been discussed elaborately in the literature[57,58]. Briefly, it can generate internally cold molecular species and therefore weakly bound complexes which are unstable at room temperature can be stabilized or synthesized and studied under collision-free conditions. Due to very low internal temperatures, very few ro-vibronic levels are populated and this greatly simplifies the spectral congestion normally observed in the room temperature samples. It also helps in categorical assignments of the observed spectral transitions.

The experimental setup consists of two differentially pumped cylindrical vacuum chambers connected by a 2 mm skimmer. The first chamber housed a sample compartment connected to a pulsed nozzle (300–500 μm diameter) that works at 10 Hz repetition rate. This chamber was dedicated to fluorescence-based measurements such as laser-induced fluorescence (LIF) and fluorescence dip IR (FDIR) spectroscopy. The fluorescence was detected by a photomultiplier tube (Hamamatsu 1P28) positioned along the axis perpendicular to the molecular beam that propagates along the cylindrical chamber axis. The molecular beam generated in the first chamber is skimmed into the second chamber that housed a time-of-flight mass spectrometer (TOFMS) with a flight tube in the direction perpendicular to the molecular beam. The complexes were laser ionized in this chamber and detected by a channeltron (Sjuts KBL25RS). One-colour or two-colour resonant two photon ionization (1c/2c-R2PI) was carried out to record mass selective electronic excitation or IR spectra.

The molecular complexes mentioned in this review involve aromatic chromophores whose S_1–S_0 excitation falls in the UV range. To investigate S_1–S_0 resonances, excitation spectra of these molecular complexes were recorded via LIF or R2PI spectroscopy[59–62]. The latter technique can provide mass selective spectral information. In the case of LIF spectroscopy, molecular complexes were excited by a tuneable UV laser and the total fluorescence from the excited state was recorded as a function of the

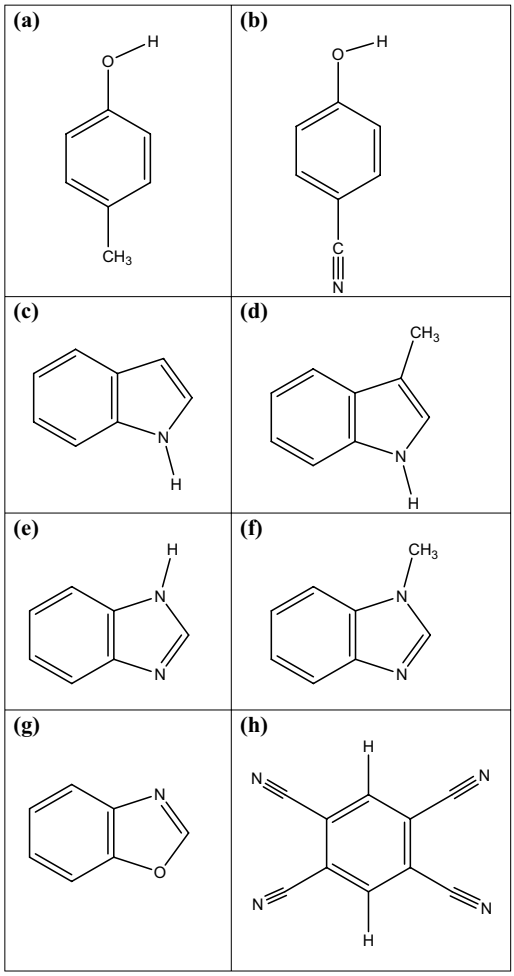

Figure 1: **a** *p*-Cresol; **b** *p*-cyanophenol; **c** indole; **d** 3-methylindole; **e** benzimidazole; **f** *N*-methylbenzimidazole; **g** benzoxazole; **h** 1,2,4,5-tetracyanobenzene.

excitation laser frequency. On the other hand, in case of 1c/2c-R2PI spectroscopy, the molecular complexes were excited to its S_1 state by a tuneable UV laser and subsequently ionized using either the same laser source (1c-R2PI) or a different UV laser source (2c-R2PI) which was temporally and spatially overlapped with the first UV laser at the molecular beam. The R2PI spectra were recorded by plotting the total ion current as a function of frequency of the excitation laser. In order to record vibrational spectra of the molecular complexes, FDIR or RIDIR spectroscopy was employed. To record a FDIR/RIDIR spectrum, a tuneable IR laser was spatially overlapped with the UV laser whose frequency was set to a particular S_1–S_0 transition. The IR pulses were synchronized to arrive 50 ns prior to the UV pulses. Whenever the IR laser frequency is in resonance with a vibrational level of the ground electronic state, the population in the zero point level decreases either due to the vibrational excitation or IR predissociation. This leads to the depletion in either total fluorescence or ion current. Therefore, the dips in the plot of total fluorescence/ion current vs IR frequency indicate vibrational resonances of the probed species.

The UV laser used for the above-mentioned spectroscopies was a frequency doubled output of tuneable dye laser which was pumped by the second harmonic (532 nm) of Nd^{3+}:YAG laser (Quantel YG-781C + TDL70). The tuneable IR source was a $LiNbO_3$-based optical parametric oscillator (OPO; LaserVision) with a line narrowing etalon. The OPO was also pumped by 1064 nm output of a Nd^{3+}:YAG laser (Quantel Brilliant-B). Both the lasers worked at 10 Hz repetition rate. Temporal synchronization of the lasers and gas pulses was controlled by an electronic delay generator (SRS-DG535). TOF–MS used in all the cases was of the Wiley–McLaren type[63]. The calibration of the IR-OPO laser was done by recording photoacoustic spectra of water, CH_4, and NH_3 and comparing them with the standard spectra provided by the HITRAN database[64]. The samples of the molecules of interest were heated to requisite temperatures to get sufficient vapour pressure which were then co-expanded with either pure helium or a pre-mixture of helium with different solvents of interest to prepare molecular complexes in the free jet.

3 Computational Methods

To get more insight into the interaction, ab initio and DFT quantum chemical calculations were performed. Geometry optimizations of several intuitionally predicted conformers of the complexes were carried out using different DFT functionals such as M06-2X, ωB97X-D, LC-ωPBE, PW1Pw91, and post Hartree–Fock MP2 levels of theory. The computations were performed using both Pople type 6-311++G** and Dunning type aug-cc-pVDZ basis sets. The harmonic frequency calculations of the optimized structures were performed at the same level of theory to get IR spectra of the optimized conformers, which were scaled with appropriate scaling factors to compare computed spectra with the experimental spectra. The optimizations of the global minimum energy conformers were mostly carried out on the counterpoise corrected surfaces (denoted by a prefix 'cp' to the respective computational level) to minimize the basis set superposition error (BSSE).

Wherever the geometry optimizations were carried out using normal gradient surfaces, the BSSE calculation were carried out separately on the optimized geometries of the complexes. The binding energies (BEs) of the complexes reported here are all zero point energy (ZPE) and BSSE corrected. All the calculations were performed using Gaussian 03/09 suite of programs[65]. To get further insight into the C–H···Y H-bonds, the wave functions of the complexes obtained from ab initio/DFT calculations were further analysed using the quantum theory of atoms in molecules (QTAIM) and natural bond orbital (NBO) analyses. QTAIM characterizes covalent and noncovalent bonds in terms of topological parameters such as electron density (ρ) and Laplacian of the electron density ($\nabla^2\rho$) at the bond critical points (BCP). The QTAIM was performed using AIM 2000 suite of programs[66]. The values of ρ in the range of 0.002–0.034 au and $\nabla^2\rho$ of 0.024–0.139 au at the bond critical point were taken as the criteria for the hydrogen bond formation as proposed by Popelier[67]. On the other hand, the NBO method was used to transform the delocalized molecular orbitals to localized molecular orbitals by unitary transformation. This approach helps a chemist to understand the electron distribution in terms of occupancy of the bonding and antibonding orbitals. The extent of interaction can be viewed as an orbital overlap and the corresponding second-order perturbation energy. The NBO analyses were performed using NBO 5.0/NBO 6.0 linked with the Gaussian 9 suite of programs[68,69]. Since H-bond is an admixture of many interactions, different components of the binding energies were calculated using natural energy decomposition analysis (NEDA). It provides the components of the of H-bonding interaction energy such as charge transfer (E_{ct}), static (E_{es}), exchange (E_{ex}), polarization (E_{pol}), and repulsive core (E_{core}) energy. It also provides NEDA energy which is basically interaction energy without dispersion interaction (E_{int}). Dispersion energy is deduced by subtracting (E_{int}) from the electronic BE calculated by MP2 or dispersion-corrected ωB97X-D method. NEDA was performed by incorporating NBO 5.0/NBO 6.0 in GAMESS, USA[70].

4 Red, Blue, and Zero Shifted C–H···Y Hydrogen Bond

It has been found that the C–H moiety activated by adjacent electronegative/electron withdrawing atom/groups is prone to hydrogen bond formation with HB acceptors. In this review, three different classes of activated C–H containing HB donors and their H-bonded complexes will be discussed, such as, (1) haloform molecules ($CHCl_3$, CHF_3), (2) imidazole or oxazole derivatives, and (3) 1,2,4,5-tetracyanobenzene (TCNB). In all these cases, the adjacent electronegative atoms or electron withdrawing groups make C–H more polar and help in stabilizing complexes with C–H···Y HBs. In the case of haloform molecules, three highly electronegative halogen atoms pull electron density away from C–H group and make it active towards H-bond formation. On the other hand, in imidazole or oxazole, the C(2)–H bond of these molecules is flanked between two electronegative elements (either two N atoms or one N and one O atom) that withdraw electron density from C(2)–H moiety to make it prone towards H-bond formation. In the third case, the presence of four electron withdrawing cyano groups makes the phenyl ring electron deficient that activates the CH groups and makes them potential H-bond donor. The extent of activation in haloforms, however, is more compared to that of imidazole or oxazole, because in the former case the electronegative elements are bound directly to the carbon atom of the C–H moiety. On the other hand, the four –CN groups in TCNB make two para C–H groups highly activated towards formation of C–H···Y H-bond. These examples present C–H···Y interaction that exhibit red, blue, and zero red shifted H-bonds.

5 Haloform Complexes with Aromatic Substrates

In this section, a set of haloform complexes with various aromatic substrates are presented. The substrates were chosen such that each one of them offers multiple acceptor sites for the C–H H-bond donor. The acceptor properties were modulated by selecting the substituents on the aromatic ring. The *p*-cresol (PCR) and *p*-cyanophenol (PCNP) (Fig. 1) were two phenol derivatives that have the para substituents of opposite nature. The methyl group at the para position in PCR increases π-electron density on the phenyl ring due to +I effect, while the CN group at the para position decreases π-electron density in the phenyl ring due to −I effect. In addition, both PCR and PCNP offer multiple HB acceptor sites, such as oxygen atom in the former molecule, oxygen and nitrogen atoms in the latter and the π-electron density in both the molecules which provides an opportunity to probe the propensity of CH···Y H-bond formation. In another set, the CH···Y

H-bonded complexes of haloforms with heterocyclic polyaromatic compounds were investigated to study the effect of polyaromaticity vs nitrogen centres as the H-bond acceptors.

5.1 p-Cresol and p-Cyanophenol Complexes

These complexes were investigated by Shirhatti et al.[30]. The LIF and R2PI spectra showed that the S_1–S_0 band origin transitions of the PCR complexes of $CHCl_3$ and CHF_3 of were blue shifted by 45 and 101 cm^{-1}, respectively, with respect to that of PCR monomer. The FDIR spectra recorded while probing the BO transitions of PCR monomer and its complexes are shown in Fig. 2. The FDIR spectrum of PCR–$CHCl_3$ complex (trace c) showed a strong transition in the C–H stretch region at 3044 cm^{-1}. This transition was assigned as the C–H stretch of $CHCl_3$ moiety in PCR–$CHCl_3$ complex, because this transition disappeared when the experiments were carried out with $CDCl_3$ (not shown in the figure). The C–H stretch was blue shifted by 11 cm^{-1} from the C–H stretch of $CHCl_3$ monomer which is known to be at 3033 cm^{-1}. The PCR–CHF_3 complex (trace b) showed a new transition at 3052 cm^{-1}. This weak C–H stretch transition was found to be blue shifted by 17 cm^{-1} from C–H stretch of the CHF_3 monomer.

The BO transitions for the complexes of PCNP with chloroform and fluoroform were found to be blue shifted by 112 and 110 cm^{-1}, respectively[30]. The FDIR spectra of the complexes of $CHCl_3$ and CHF_3 are also shown in Fig. 2. The FDIR spectrum of PCNP–$CHCl_3$ complex (trace f) showed intensity-enhanced strong transition at 3033 cm^{-1}, assigned as the C–H stretch of $CHCl_3$ moiety. The shift observed in the C–H stretching frequency with respect to the $CHCl_3$ monomer was zero, i.e. this is an example of zero shifted H-bond. The FDIR spectrum of PCNP–CHF_3 complex (trace e) showed the C–H stretch of CHF_3 moiety at 3062 cm^{-1} which was blue shifted by 27 cm^{-1} compared to the same in CHF_3 monomer.

Although a single conformer was observed experimentally in the above cases, computationally multiple conformers were predicted to be stable for each of them at various DFT levels of computations. However, at the MP2/aug-cc-pVDZ level, only the C–H···π bound conformers were found to be stable for the PCR–haloform complexes. The BSSE- and ZPE-corrected binding energies computed at the

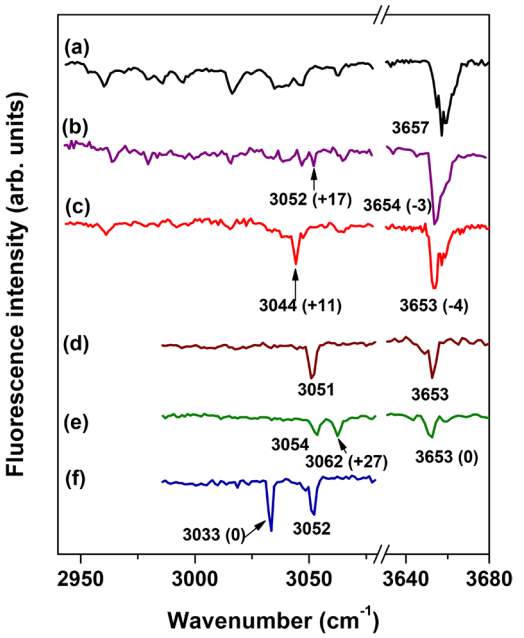

Figure 2: FDIR spectra of **a** PCR monomer and its **b** CHF_3 and **c** $CHCl_3$ complexes; FDIR spectra of **d** PCNP monomer and its **e** CHF_3 and **f** $CHCl_3$ complexes. The shifts in the C–H and O–H stretching frequencies in the complexes compared to those in the monomers are mentioned in parentheses.

MP2 as well as the *cp*-MP2/aug-cc-pVDZ level are given in Table 1. As far as the CH stretching frequency prediction was concerned, the best agreement was observed for the conformers optimized using counterpoise corrected gradients (*cp*-MP2). The C–H stretching frequency computed at the *cp*-MP2 level for the PCR–$CHCl_3$ complex gave a blue shift of 19.6 cm^{-1} which was a significant improvement over that computed at the MP2 level and was in excellent agreement with the observed blue shift of 11 cm^{-1}. The computed blue shift in the CH frequency for the PCR–CHF_3 complex was 24.8 cm^{-1} which agrees well with the observed blue shift of 17 cm^{-1}. AIM calculations of these complexes suggest the presence of BCP at the bond path of C–H–π interaction. The magnitude of the electron densities at the BCPs were 0.0152 and 0.0104 for $CHCl_3$ and CHF_3 complexes, respectively, (Table 1) which are within the specified range for the H-bonding interaction. It also showed an increase in electron density (Table 1) at the BCP corresponding to C–H bond that acts as a HB donor consistent with the observed blue shift in C–H stretching frequencies in these complexes.

Table 1: Dissociation energies (D_0) of the conformers of PCR and PCNP complexes with $CHCl_3$ and CHF_3 computed at the MP2/aug-cc-pVDZ level. Other parameters such as C–H stretch frequency shift ($\Delta\nu$), intensity enhancement ratio, change in the C–H bond length (Δr), electron density (ρ) at the H-bond critical points, and change in electron density ($\Delta\rho$) at the C–H bond critical points are also tabulated.

Parameters[a]	PCR–$CHCl_3$ CH···π	PCR–CHF_3 CH···π	PCNP–$CHCl_3$ CH···N	PCNP–$CHCl_3$ CH···π	PCNP–$CHCl_3$ CH···O	PCNP–CHF_3 CH···N	PCNP–CHF_3 CH···π	PCNP–CHF_3 CH···O
D_0/kcal/mol	5.9 (6.8)	3.5	3.9 (5.4)	4.2 (5.2)	3.7 (4.2)	3.5 (3.7)	1.7	1.8
$\Delta\nu$ (C–H)/cm^{-1}	57.3 (19.6) 11[b]	24.8 N.A. 17[b]	16.8 (−2.1) Zero[b]	65.0 (11.3)	23.2 (−0.7)	22.1 (20.2) 27[b]	17.2 N.A.	18.7 N.A.
Intensity enhancement ratio	0.1	70.5	231.8 (25.6)	44.3 (22.3)	16.5 (10.6)	1.2	0.3	0.1
Δr(C–H)/mÅ	−2.9	−1.7	−0.5	−3.7	−1.2	−1.4	−1.2	−1.2
ρ (BCP)/au	0.0152	0.0104	0.0135	0.0090, 0.0088[c]	0.012	0.0185	0.0139	0.0109, 0.0107[c]
$\Delta\rho$ (C–H)/au	0.0041	0.0032	0.0032	0.0026	0.0027	0.0027	0.0044	0.0021

[a] The numbers in parentheses in each row correspond to the results of the calculations at the *cp*-MP2/aug-cc-pVDZ level
[b] Experimental observed frequency shift
[c] Two BCPs were observed for these structures

In the case of PCNP complexes, three different conformers were predicted at the MP2/aug-cc-pVDZ level in each of the cases. These conformers are C–H···N, C–H–π, and C–H···O type. Although all the conformers showed blue shift in C–H stretch frequency (Table 1), the predicted frequencies were quite off from the observed ones for the $CHCl_3$ complexes. When the harmonic frequencies were computed for the conformers optimized using counterpoise corrected gradients (*cp*-MP2), significant improvement was noted in the corresponding frequency calculations. For example, a red shift of 2.1 and 0.7 cm^{-1} for the C–H···N and C–H···O bound complexes, respectively, and a blue shift of 11.3 cm^{-1} C–H–π bound complex were predicted. The BSSE-corrected BEs of these conformers (Table 1) indicated that the C–H···N bound conformer was the global minimum structure. Based on the relative BE, the C–H···N bound conformer was assigned as the observed conformer for PCNP–$CHCl_3$ complex which is a zero shifted complex, i.e. CH stretching frequency showed a zero shift. Similar results were reported by Mikami et al. in the case of benzonitrile–$CHCl_3$ complex[49]. The report also emphasised that counterpoise gradient calculation is important for good prediction of vibrational frequency in such complexes. Similarly, for PCNP–CHF_3 complex, the C–H···N bound conformer was predicted to be the global minimum. The harmonic frequency calculation predicted the blue shift of 20.2 cm^{-1} for the global minimum structure, in good agreement with the observed blue shift of 27 cm^{-1}. Based on relative BEs of the conformers, C–H···N HB bound structure was assigned as the observed conformer.

These results illustrated the effect of *p*-substitution on the mode of interactions in substituted phenol–haloform complexes. The methyl group in PCR enhances the electron density on the π-cloud of the aromatic ring and facilitates the formation of C–H–π HB instead of other type of HBs. A strong electron withdrawing group causes depletion of electron density in the aromatic π-electron density thereby destabilizing C–H–π interaction with respect to the C–H···N HB in the complexes of PCNP–haloform complexes.

5.2 3-Methylindole (MI) Complexes

3-Methylindole (Fig. 1) presents an example of heterocyclic polyaromatic compound. The bicyclic aromatic substrate provides a large surface with π electron density. The NH group in the five-member ring provides an alternative H-bond donor group. The LIF as well as the 2c-R2PI spectra confirmed that the BO transition of MI–$CHCl_3$ showed a red shift of 23 cm^{-1} compared to that of the BO transition of the monomer[31]. The BO transition of the complex was probed by FDIR spectroscopy to interrogate the binding site for the haloform CH donor molecule. The FDIR spectra of the MI monomer, MI–$CHCl_3$, and MI–CHF_3 complexes are shown in Fig. 3. The strong transition observed at 3035 cm^{-1} in the FDIR spectrum of MI–$CHCl_3$ complex was assigned

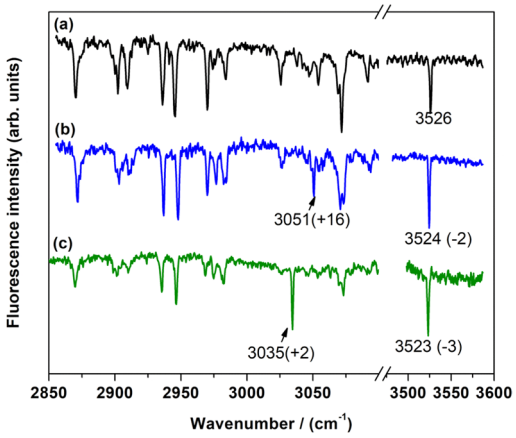

Figure 3: FDIR spectra of **a** MI, **b** MI–CHF_3, and **c** MI–$CHCl_3$ complexes in the CH and N–H stretch regions. The arrows indicate the positions of the hydrogen bonded C–H stretch transition of the haloform moieties in the complexes. The shifts in the C–H and N–H stretching frequencies in the complexes compared to those in the monomers are mentioned in parentheses.

as the CH stretching frequency of $CHCl_3$ in the complex, as it was absent both in MI monomer as well as MI–$CDCl_3$ complex (not shown in the figure). The C–H stretch transition of $CHCl_3$ moiety in MI–$CHCl_3$ was blue shifted by 2 cm^{-1}. Similarly, MI–CHF_3 complex was also probed using LIF and FDIR spectroscopy. The electronic BO transition for this complex was found to be blue shifted by 7 cm^{-1}. The FDIR spectrum of MI–CHF_3 complex (Fig. 3b) shows the C–H stretch transition of CHF_3 moiety. The transition observed at 3051 cm^{-1} which was blue shifted by 16 cm^{-1} compared to C–H stretch in CHF_3 monomer.

Computationally two different conformers were predicted for the MI–$CHCl_3$ complex at the MP2/6-311++G** level out of which the C–H–π bound conformer was the global minimum. In the other conformer, CH pointed away from the aromatic surface. For the MI–CHF_3 complex, only a single conformer, i.e. the C–H–π bound conformer was optimized. In both the cases, the C–H group points toward the π-cloud of the phenyl ring. BSSE- and ZPE-corrected binding energies of the global minimum energy conformers are given in Table 2. Comparison of the IR spectra and BE calculations of the conformers suggests that both $CHCl_3$ and CHF_3 complexes form C–H–π type conformer in the molecular beam. As far as the predicted CH stretching frequencies of the complexes were concerned, the agreement with the observed frequencies was not so good but the IR transition probabilities agreed very well. The computation of frequencies needs to be carried out for the structures optimized on the counterpoise corrected surface for better agreement.

Dispersion interaction was considered initially as one of the key factors for blue shifted H-bonds[47,50]. It was explained that due to attractive nature of dispersion interaction, HB donor and acceptor came very close to each other within the repulsive regime which causes blue shift of C–H stretch. The extent of dispersion contribution in the MI–haloform (C–H–π bound complexes) has also been reported and compared with the existing literature data as shown in Table 2. It can be seen that in general the C–H–π bound complexes are dominated by the dispersion interaction and the contribution of the dispersion interaction to the total interaction is at times more than 100%[71–73]. However, the dispersion effect cannot solely explain the blue shifting nature of the C–H···Y H-bond. There are reports which showed that blue shifting can be shown even with Hatree–Fock level of calculation which does not take into account the dispersion interaction[54,74].

Insofar, in the complexes presented above, it is observed that the extent of blue shift is always higher for CHF_3 complex than that the $CHCl_3$ complex. This is similar to the trend reported by van der Veken et al.[32,33] who found that the blue shift in the C–H stretch frequency progressively increases with the number of F atoms in $CHF_nCl_{(3-n)}$ moiety in the $CHF_nCl_{(3-n)}$–X (X=O-containing solvents) complexes. They also observed that the IR intensity also decreased with the number of F atoms and IR intensity is minimum for CHF_3 complex and maximum for $CHCl_3$ complex. This is consistent with the intensity trend observed in the results presented above.

5.3 7-Azaindole Complexes

As another example of heterocyclic polyaromatic compound, the haloform complexes of 7-azaindole (Fig. 1) were investigated by Shirhatti et al.[75]. The reports on the C–H···O or C–H···π systems in cold matrices, cryo solutions, and in cold molecular beams are quite abundant[32–35,48,76–79], but the studies of C–H···N interaction in the literature are rare, barring a few examples investigated using IR absorption spectroscopy[80–86]. In addition, 7-azaindole also offers multiple possibilities for the formation of complexes with haloforms. For example, π electrons of both the rings and N atoms of 7-azaindole can act as a HB

Table 2: Dissociation energies (D_0), dispersion energy (E_{corr}), % dispersion component for the complexes of MI with $CHCl_3$ and CHF_3 at MP2/6–311++G** level. Other parameters such as C–H frequency shift ($\Delta\nu$), IR intensity enhancement ratio, change in C–H bond length (Δr), electron density (ρ) at the H-bond critical point, change in electron density ($\Delta\rho$) at the C–H bond critical point are also tabulated. $E_{corr} = (D_0 - D_0^{HF})$, % dispersion $= (E_{corr}/D_0) \times 100$, $D_0^{HF} = D_0$ estimated at HF level. The table also includes % dispersion of some other reported C–H–π bound complexes.

Parameters	3-Methylindole–CHF_3	3-Methylindole–$CHCl_3$
D_0/kcal/mol	4.17	5.91
E_{corr}/kcal/mol	1.76	3.81
% Dispersion	42	64
$\Delta\nu$ (C–H)/cm^{-1}	22	39
	16[a]	2[a]
Intensity enhancement ratio	0.2	7000
Δr(CH)/mÅ	− 1.93	− 1.71
ρ (BCP at H···Y)/au	0.0095	0.0132
$\Delta\rho$ (BCP at C–H)/au	0.0033	0.0037
Parameters	**Benzene–methane[b]**	**Indole–methane[c]**
D_0/kcal/mol	1.52	2.29
E_{corr}/kcal/mol	2.67	5.49
% dispersion	176	240
Parameters	**Benzene–chloroform[d]**	**Benzene–fluoroform[d]**
D_0/kcal/mol	5.60	4.20
E_{corr}/kcal/mol	7.90	3.40
% dispersion	141	81

[a] Experimentally observed frequency shift
[b] D_0 estimated at the CCSD(T), basis set limit (ref.[71])
[c] D_0 estimated at the MP2, basis set limit (ref.[72])
[d] D_0 estimated at the CCSD(T), basis set limit (ref.[73])

acceptors. On the other hand, N–H site can act as a HB donor for the halogen atoms.

Mass selective 1c-R2PI spectra of the AI monomer and its haloform complexes showed that the BO transitions were red shifted upon complex formation for both the complexes. The red shift in electronic BO for $CHCl_3$ complex was found to be 309 cm^{-1}, whereas the same for the CHF_3 complex was 243 cm^{-1}. The BO transitions of the AI–$CHCl_3$ and AI–CHF_3 complexes were probed by FDIR spectroscopy as shown in Fig. 4. An unusually broad and strong transition was observed at 2951 cm^{-1} in the case of the $CHCl_3$ complex (trace b) and it was assigned as the C–H stretch transition $CHCl_3$ in the complex. This assignment was confirmed by performing FDIR experiments of AI–$CDCl_3$ complex wherein this feature disappeared (trace c). The C–H stretching frequency of $CHCl_3$ moiety in the AI–$CHCl_3$ complex showed a red shift of 82 cm^{-1} with respect to that of $CHCl_3$ monomer. On the other hand, FDIR spectrum of AI–CHF_3 (trace d) showed that C–H stretch of CHF_3 in this complex appeared at 3039 cm^{-1} which was blue shifted by 4 cm^{-1} with respect to that for CHF_3 monomer. The FDIR spectra were also recorded in the NH stretching region. It was reported that the NH stretching frequency was also affected in the complexes significantly, i.e. in the $CHCl_3$ and CHF_3 complexes, the NH stretching frequency was red shifted by 56 and 22 cm^{-1}, respectively. This indicates that in the AI–haloform complexes both CH as well as NH are involved in the complex formation.

Computationally four different conformers have been optimized for the AI–$CHCl_3$ complex. The respective zero point energy corrected

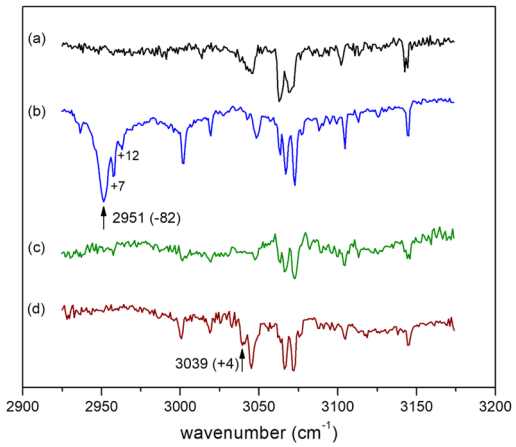

Figure 4: FDIR spectra **a** 7-AI, **b** 7-AI:$CHCl_3$, **c** 7-AI:$CDCl_3$, and **d** 7-AI:CHF_3 in the C–H stretch region. The C–H transition of the CHX_3 moiety in the complexes has been marked by arrows. The magnitudes of shifts in the C–H stretch frequency upon complex formation are given in the parentheses. Reprinted with permission from Ref.[75]. Copyright © 2014 WILEY–VCH Verlag GmbH & Co. KGaA, Weinheim.

binding energies are given in Table 3. In all these conformers, C–H of $CHCl_3$ acts as a HB donor, however, among these four conformers, C–H···N bound planar conformer was found to be the global minimum energy conformer at the MP2/aug-cc-pVDZ level of theory. On the other hand, geometry optimization of the AI–CHF_3 complexes suggested three different conformers (Table 3). Even in this case, the C–H···N bound planar conformer was the global minimum energy conformer. Computed harmonic frequency calculations of the AI–$CHCl_3$ complexes suggested red shifts of 102.5 cm^{-1} for planar conformer. From both BE viewpoint and frequency agreement with the experimental IR spectrum, it was quite straightforward to assign the C–H···N HB bound planar conformer to be the observed conformer for AI–$CHCl_3$ complex. However, the calculated IR spectra of the AI–CHF_3 complexes predicts a red shift of 25.6 cm^{-1} for C–H···N HB bound planar conformer and blue shifts of 17.2 and 0.1 cm^{-1} for C–H···π pyridyl, and C–H···π pyrrole complexes, respectively. In this case, there was a bit of dichotomy in the relative binding energies and the agreement between the observed and computed CH stretching frequency shifts. Once again, the frequency calculations were refined using the counterpoise corrected surface. The counterpoise gradient corrected CH and NH frequency red shifts for the $CHCl_3$ complex were 94 and 44 cm^{-1}, respectively, in excellent agreement with the observed frequency shifts while those for the N-bound planar CHF_3 complex were 9 and 22 cm^{-1}, respectively. For the CHF_3 complex, computations at various DFT levels were also tried to reproduce the blue shift in the CH stretching frequency without any avail. Assigning the observed conformer to the π-bound conformer in this case based on the computed blue shifted CH frequency, however, was not consistent with the observed large red

Table 3: Dissociation energies (D_0) for AI–$CHCl_3$ and AI–CHF_3 conformers computed at the MP2/aug-cc-pVDZ level. Other parameters such as frequency shift (Δν (C–H)), frequency shift (Δν (N–H)), change in C–H bond length (Δ*r*), and electron density (ρ) at the H-bond critical point are also tabulated.

	AI–$CHCl_3$				AI–CHF_3		
Parameters	C–H···N (planar)	C–H···N (perp.lar)	C–H···π (pyridyl)	C–H···π (pyrrole)	C–H···N (planar)	C–H···π (pyridyl)	C–H···π (pyrrole)
D_0/kcal/mol	6.46	6.27	5.69	5.41	5.06	3.34	2.88
Δν (C–H)/ cm^{-1}	−102.1	−48.5	53.9	42.9	−25.6	17.2	0.1
	−94.4[a]	−42.9[a]	N.A.	N.A.	−8.5[a]	N.A.	N.A.
	−82[b]	–	–	–	4[b]	–	–
Δν (N–H)/ cm^{-1}	−54.4	−17.0	−5.1	−11.1	−23.1	−−2.9	−10.0
	−43.8[a]	−15.4[a]	N.A.	N.A.	−21.6[a]	N.A.	N.A.
	−56[b]	–	–	–	−22[b]	–	–
Δ*r*(CH)/mÅ	6.5	3.1	−2.7	−2.3	1.4	−1.1	−0.1
ρ (BCP at H···Y)/au	0.0252	0.0210	0.0131, 0.0132[c]	0.0161	0.0175	0.0092, 0.0093[c]	0.0105

[a] Calculated at *cp*-MP2/aug-cc-pVDZ level
[b] Experimentally observed frequency shift
[c] Two BCPs were observed

shift in the electronic BO of the observed conformer. It is well documented in the literature that the π-bound conformers invariably show large blue shifts in the electronic band origin. For example, Zwier et al.[87] have reported blue shifts of 52 and 152 cm^{-1} for the transition 6_0^1 in the π-bound complexes of benzene with H_2O and HCl, respectively. Fujii et al.[88] have reported that the C–H–π bound complexes of benzene with $CHCl_3$ and CH_2Cl_2 showed blue shifts of 178 and 105 cm^{-1}, respectively, in the 6_0^1 (S_1–S_0) transitions. Based on these arguments, the observed conformer for AI–CHF_3 was assigned as the CH···N bound planar conformer based on the computed binding energy and the observed large red shift in the electronic band origin transition. The discrepancy of 4 cm^{-1} blue shift was explained as shifting in energy levels due to Fermi resonance between the C–H stretching vibration with the overtones of C–H bend vibrations in analogy with the reported pseudo-blue shift in the case of the CHF_3–pyridine complex[82].

The observed large red shift in the CH stretching frequency in the case of AI–$CHCl_3$ complex is consistent with those reported in the literature for the other CH···N bound complexes as given in Table 4. It can be seen that the C–H···N bound $CHCl_3$ complexes always showed red shifts in C–H stretch transition. However, C–H···N bound CHF_3 complexes can show either a red shift or blue shift depending upon the experimental conditions or the systems studied. Although the calculated BE at the MP2 level for AI–$CHCl_3$ (6.46 kcal/mol) and large CH stretch red shift (82 cm^{-1}) indicate that the C–H···N H-bond in this complex is quite comparable to the conventional H-bonds, it is pointed out that the net binding energy in this case may not be solely due to the CH···N interaction, i.e. it must also have the contribution from the NH···Cl/F interaction. On the other hand, AI–CHF_3 complex showed a small blue shift (4 cm^{-1}) unlike conventional H-bonds, but the BE (5.06 kcal/mol) of this complex was also found to be quite high and comparable to the AI–$CHCl_3$ complex.

In all the cases, the extent of observed blue shifts was more in the fluoroform complexes than the corresponding chloroform complexes. It can be noted that C–H stretch of $CHCl_3$ showed red, zero, and blue shifts in the complex of AI–$CHCl_3$, PCNP–$CHCl_3$ complex, and (MI–$CHCl_3$ and PCR–$CHCl_3$), respectively. These results emphasised the role of HB acceptors in determining the direction of the C–H stretch shifts.

6 Imidazole/Oxazole Complexes

In this section, spectroscopic behaviour and role of the moderately activated C–H moieties will be discussed. Imidazole moiety is an important biological entity that is not only an integral part of many crucial biological molecules such as amino acids, nucleobases, and alkaloids,[89] but it is also actively involved in controlling functions of these biological molecules. Imidazole group is an interesting system to investigate the role of the C–H···Y H-bonds in biological systems, as it possesses a moderately activated C(2)–H bond along with inherent conventional HB donor (N–H bond) and acceptor [lone pair (lp) of N] sites. Active participation of this activated C(2)–H bond in C–H···O H-bond is known in the literature. For example, C(2)–H of imidazole group forms C–H···O H-bond with adjacent >C=O group of peptide backbone in a catalytic triad that plays a crucial role in certain enzymatic reactions[18]. It is also found as a potential HB donor in molecular crystals[90] and ionic liquids[91], Bhattacherjee et al.[92]–[95] have cleverly chosen imidazole containing organic systems such as benzimidazole (BIM)/1-methylbenzimidazole (MBIM) (Fig. 1) where the C(2)–H of imidazole moiety is decoupled from rest of the C–H stretch of the systems. Therefore, C(2)–H of imidazole acts as a local oscillator and hence finds it easy to distinguish its stretching transition in the respective vibrational spectra. The other system of interest is O-analogue of BIM which is benzoxazole (BOX). Like imidazole, oxazole is another natural constituent of alkaloids, oligosaccharides, and vitamins[89].

Mass gated electronic excitation spectrum of 1:1 complex of BIM–W_1 (W = water) showed three transitions in the electronic excitation spectrum[92]. One of them was red shifted by 68 cm^{-1} compared to the BO of BIM monomer, whereas the other two showed blue shifts of 104 and 149 cm^{-1}. On the other hand, electronic excitation spectrum of mass gated MBIM–W_1 showed only two transitions which were blue shifted by 117 and 193 cm^{-1}. Similar to MBIM–W_1, BOX–W_1 also showed only two transitions in the electronic excitation spectrum[94]. One of them was red shifted by 27 cm^{-1}, whereas the other transition was blue shifted by 91 cm^{-1}. Structural information of the complexes corresponding to these transitions was envisaged with the help of experimental and computed IR spectra. The C(2)–H stretch of BIM appeared at 3095 cm^{-1}, and the same for MBIM appeared at 3103 cm^{-1}. The intensities of the C(2)–H stretch transitions were very weak. The C(2)–H transition for BOX was so weak that it could

Table 4: A summary of reported experimental frequency shifts of the C–H stretch transition in various C–H···N bound complexes.

Complex	Shift in C–H stretch of HB donor (cm^{-1})	Experimental method	Remarks
$CHCl_3$: NH_3[a]	−38	Supersonic Jet FTIR	Jet temperature
$CHCl_3$: NH_3[b]	−17.5	Gas phase FTIR	Room temperature
$CHCl_3$: NH_3[c]	−45	Ar matrix	20 K
$CHCl_3$: NH_3[c]	−94	N_2 matrix	20 K; broad peak
CHF_3: NH_3[d]	+7.6	Liq Xe	188 K
CHF_3: NH_3[d]	−21	Ar matrix	20 K
CHF_3: NH_3[c]	−45	N_2 matrix	20 K
$CHCl_3$: NMe_3[e]	−105	Liq Kr	120 K
F_2ClCH: NMe_3[e]	−32	Liq Kr	120 K
CHF_3: NMe_3[d]	−22.8	Liq Ar	90 K
$CDCl_3$:NH_3[f]	−12	Gas phase IR	Room temperature
$CDCl_3$:$MeNH_2$[f]	−26	Gas phase IR	Room temperature
$CDCl_3$:Me_2NH[f]	−45	Gas phase IR	Room temperature
$CDCl_3$: NMe_3[f]	−53	Gas phase IR	Room temperature
CHF_3:Pyridine[d]	+3	Liq Xe	188 K
$CHCl_3$:7-Azaindole[g]	−82	IR-UV jet	Jet temperature
CHF_3:7-Azaindole[g]	+4	IR-UV jet	Jet temperature

[a] Reference[85]
[b] Reference[84]
[c] Reference[86]
[d] Reference[82]
[e] Reference[81]
[f] Reference[80]
[g] Reference[75]

not be observed in the respective IR spectrum. The IR spectra of all the conformers also did not show any significant activity in the CH stretching frequency, but the NH stretching frequency of BIM and the OH stretching frequencies of the solvent molecule, viz., water showed significant shifts. Comparison of FDIR spectra and computed IR spectra of the complexes suggested that the red shifted electronic transition for BIM–W_1 corresponds to a N–H···O bound conformer, whereas the blue shifted electronic transitions of all the complexes (BIM–W_1, MBIM–W_1 and BOX–W_1) correspond to O–H···N bound conformers where water molecule was tilted to either the phenyl ring or the imidazole ring as shown in Fig. 5. The absence of any activity in the C–H region of the spectra of all these conformers compared to the same for the respective monomers indicated that the C(2)–H does not play any role in stabilizing the 1:1 complexes.

6.1 BIM/MBIM/BOX–W_n ($n > 1$) Complexes

Although C(2)–H group was not found to play any role in the 1:1 complexes of BIM/MBIM/BOX with water, it was found that the CH group actively participates in H-bonding in higher water complexes[95]. The electronic excitation spectra of the higher complexes of BIM/MBIM with water (1:n where $n > 1$) showed a single conformer for each of the cases. Figure 6 shows the FDIR spectra of BIM–W_n ($n = 2$–4) complexes along with closely matched computed IR spectra. FDIR spectrum of BIM–W_2 complex showed that the N–H stretch transition position remains unchanged, i.e. N–H of BIM does not participate in the H-bonding. Interestingly, C(2)–H stretch transition was found to be blue shifted by 14 cm^{-1} and the IR intensity enhancement of the order of sixfold over that of the monomer was observed which clearly suggests that C(2)–H of BIM actively participates in H-bonding to stabilize this 1:2 complex. The transitions observed above 3200 cm^{-1} were due to the bound and free O–H

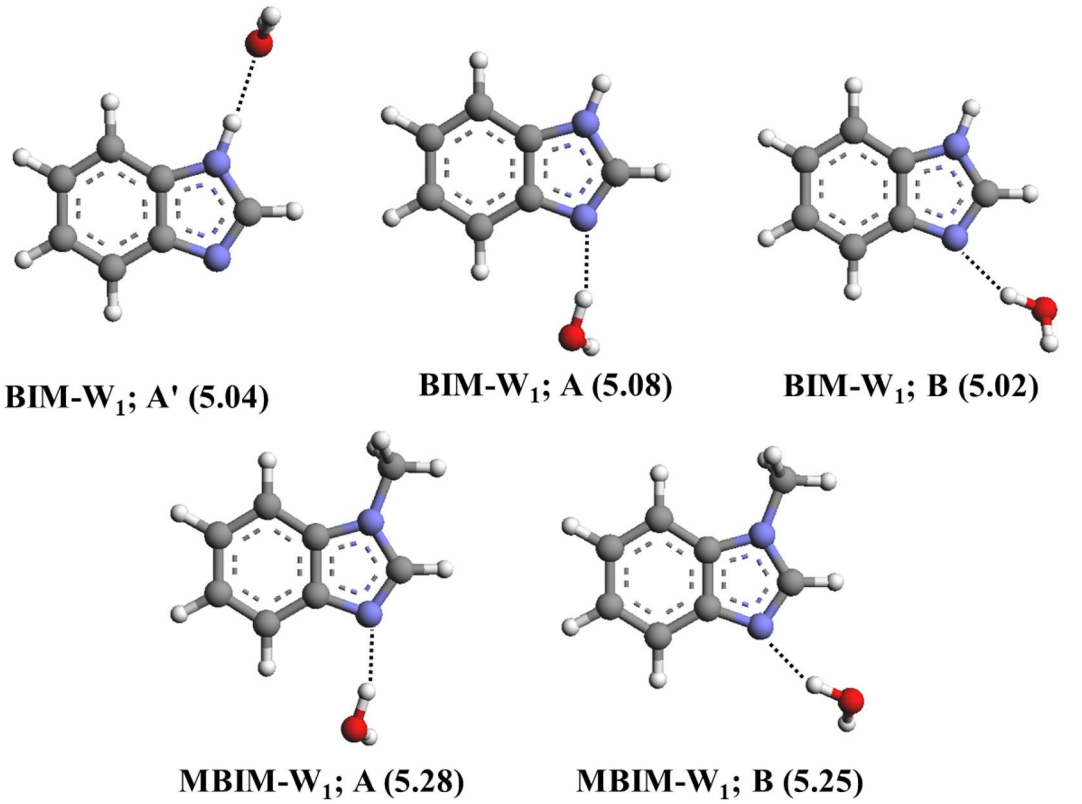

Figure 5: Optimized global minimum energy conformers whose IR spectra closely matched with the observed FDIR spectra of BIM–W_1 and MBIM–W_1 complexes at the *cp*-MP2/aug-cc-pVDZ level. The number in the parentheses indicate the computed BE in kcal mole^{-1}. The conformer A' of BIM-W_1 corresponds to the red shifted BO band and the A, B conformers for BIM–W_1 and MBIM–W_1 correspond to the blue shifted BO band in the respective LIF spectra. Reference[92]—reproduced by permission of the PCCP Owner Societies.

stretches of water. Experimental IR spectrum was best reproduced by the calculated IR spectrum of the conformer that has two water molecules forming a hydrogen bonded water chain bound to the imidazole moiety via O–H···N HB with the N centre of imidazole and a $C(2)-H\cdots O_{H_2O}$ HB in a seven-membered cyclic ring structure as shown in Fig. 7. This result clearly highlights that C(2)–H···O HB does play an active role in building up the water complexes around BIM. This conformer was also found to be the global minimum structure at various levels of theory[95]. In an earlier report, Simons et al.[96] have reported that in the case of dihydrated complex of 4-phenylimidazole (another derivative of imidazole), water molecules form a hydrogen bonded bridge structure between N–H site and the π-aromatic cloud of the imidazole ring. However, such a structure was not observed for BIM–W_2 by Bhattarcherjee et al.[95]. In case of BIM–$W_{3,4}$, FDIR spectra did not show any IR intensity enhancement for C(2)–H stretch transition and the experimental FDIR spectra were nicely reproduced by the calculated IR spectra of the conformers having a water bridge structure between N centre and N–H centre of BIM and indicated that the $C(2)-H\cdots O_{H_2O}$ H-bond cannot compete energetically with the NH···O interaction in stabilizing these higher complexes. However, when the NH site in BIM is methylated as in MBIM, the role C(2)–H···O HB in stabilizing higher water complexes was evident. The FDIR spectrum of MBIM–W_2 (Fig. 8) also showed that IR intensity enhancement for C(2)–H stretch mode was almost tenfold. The conformer whose calculated IR spectrum agreed with the experimental spectrum was a structure in which a hydrogen bonded water chain was anchored between N centre and C(2)–H of MBIM via the O–H···N and $C(2)-H\cdots O_{H_2O}$ H-bonds, respectively (Fig. 7). This conformer was also found to be the global

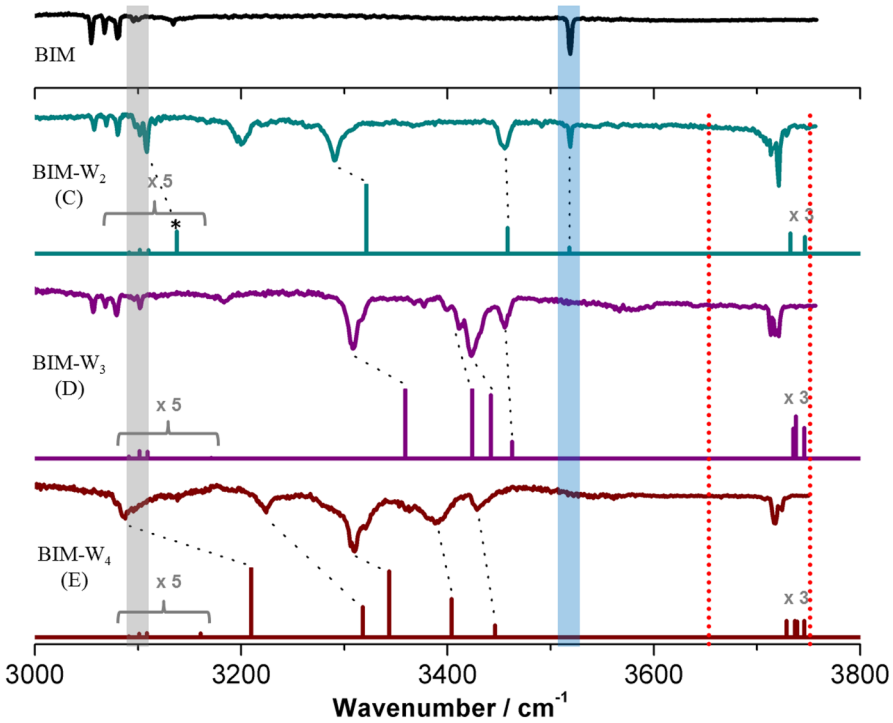

Figure 6: FDIR spectra of BIM monomer and its W_n (n=2–4) clusters and corresponding closely matched scaled computed (*cp*-MP2/aug-cc-pVDZ) IR spectra are shown for comparison. The red dotted lines indicate the position of the symmetric and antisymmetric stretch mode of free water monomer. The blue and grey shaded bars indicate the position of N–H stretch and C(2)–H stretch of BIM monomer, respectively. The asterisk in the computed spectra of BIM–W_2 indicates the intensity enhancement of the C(2)–H stretch transition in this complex. The black dotted lines indicate the correspondence between experimental and computed transitions. Reference[95]—reproduced by permission of the PCCP Owner Societies.

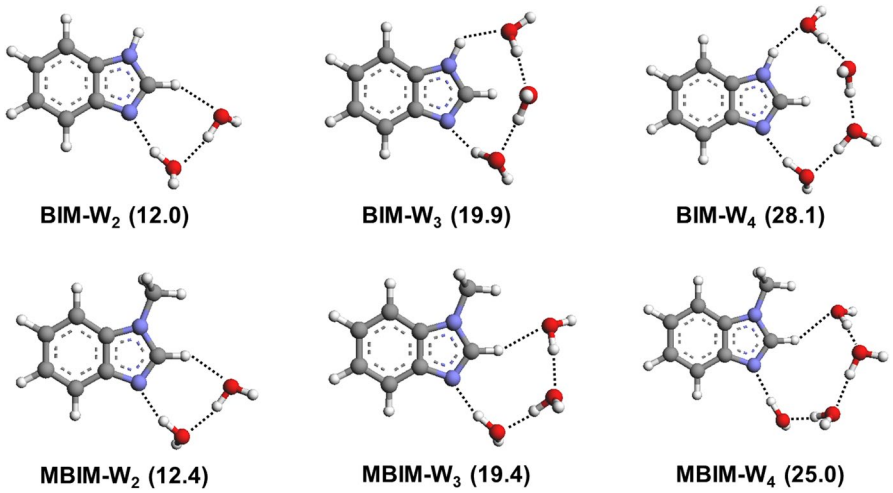

Figure 7: Optimized global minimum energy structures for BIM-W_n (n=2–4) and MBIM–W_n (n=2–4) at *cp*-MP2/aug-cc-pVDZ. The numbers in the parentheses indicate their calculated BE in kcal mole^{-1}. Reference[95]—reproduced by permission of the PCCP Owner Societies.

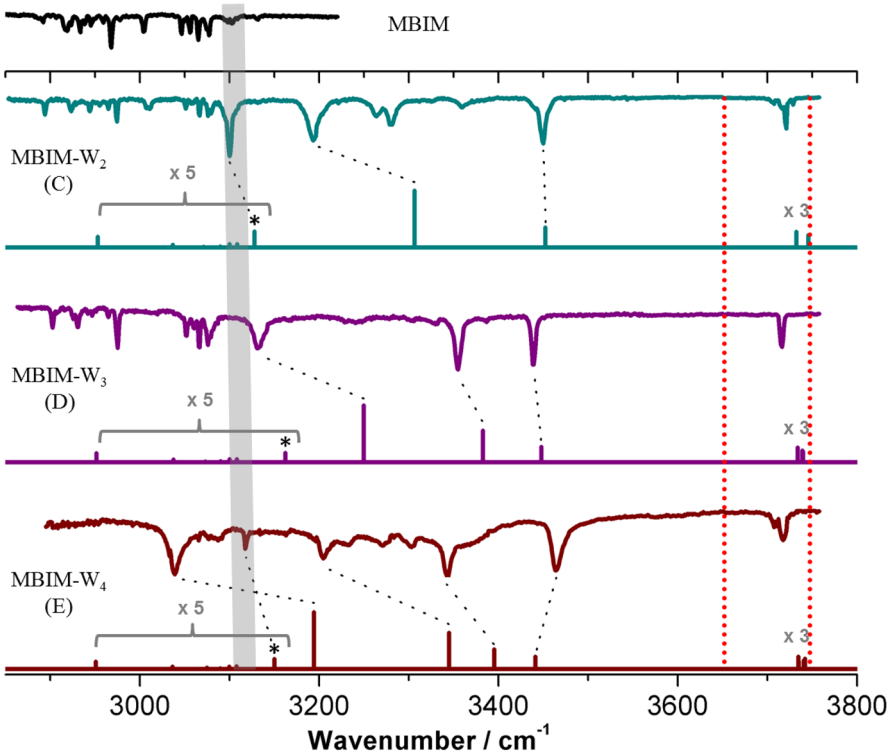

Figure 8: FDIR spectra of MBIM monomer and MBIM–W_n (n=2–4) clusters and corresponding closely matched scaled computed (*cp*-MP2/aug-cc-pVDZ) IR spectra are shown for comparison. The red dotted lines indicate the position of the symmetric and antisymmetric stretch mode of free water monomer. The grey shaded bar indicates the position of C(2)–H stretch of MBIM monomer. The transitions marked by asterisks are assigned as the C(2)–H stretch transition. The black dotted lines indicate the correspondence between experimental and computed transitions. Reference[95]—reproduced by permission of the PCCP Owner Societies.

minimum energy structure according to various dispersion-corrected DFT functionals as well as MP2 level of theory. Not only the MBIM–W_2 complex but MBIM–$W_{3,4}$ was also found to have a water bridge structure between N centre and the C(2)–H moiety unlike BIM–$W_{3,4}$ complexes. These results clearly indicate that whenever the N centres of the imidazole are unavailable for interaction, the activated C(2)–H participates in H-bonding. The BEs of the MBIM–$W_{3,4}$ were comparable to that of the BIM–$W_{3,4}$ complexes suggesting that the stabilization provided by the $C(2)-H\cdots O_{H_2O}$ H-bond in the MBIM–$W_{3,4}$ must be comparable to the $N-H\cdots O_{H_2O}$ HB in the BIM–$W_{3,4}$ complexes.

In case of BOX, the highest water complex consisted of only two water molecules and only single conformer of BOX–W_2 complex was observed in the LIF and 2c-R2PI spectra[94]. The FDIR spectrum showed an enhancement of the IR transition intensity for the transition at 3120 cm^{-1} which has been assigned as the C(2)–H stretch transition of BOX indicating its involvement in H-bonding. Comparison between the experimental spectrum and the computed spectra indicated that the observed conformer corresponds to the one that has hydrogen bonded water bridge between N centre and C(2)–H moiety of BOX molecule, very similar to BIM/MBIM–W_2 complexes.

The interaction of C(2)–H group of BIM/MBIM/BOX was also probed in the complexes of other oxygen containing protic solvents with higher proton affinities than water, namely, methanol and ethanol by Bhattacherjee et al.[93] using LIF, 2c-R2PI, and FDIR spectroscopy. With the help of calculated IR spectra and experimental FDIR spectra, it was found that the 1:1 complexes with alcohols did not show any activity in the C–H region, i.e. the C(2)–H did not participate in any interactions to stabilize these conformers, similar to BIM/MBIM–W_1 complexes[92]. FDIR spectrum of BIM–M_2 (M = methanol), however, showed that the intensity of the C(2)–H stretch transition was enhanced by sevenfold indicating the involvement of the C(2)–H in H-bonding

Table 5: Computed dissociation energies (D_0) of the experimentally observed conformers of BIM, MBIM, and BOX complexes in kcal/mol.

Level/basis set	BIM–W_1	BIM–W_2	BIM–W_3	BIM–W_4
cp-MP2/aug-cc-pVDZ	5.04, 5.08, 5.02	12.0	19.9	28.1
cp-MP2/aug-cc-pVDZ	MBIM–W_1	MBIM–W_2	MBIM–W_3	MBIM–W_4
	5.28, 5.25	12.4	19.4	25.0
MP2/aug-cc-pVDZ	BIM–M_1	BIM–M_2	–	–
	5.87	14.48	–	–
MP2/aug-cc-pVDZ	MBIM–M_1	MBIM–M_2	MBIM–M_3	–
	6.14	14.85	23.30	–
cp-MP2/aug-cc-pVDZ	BOX-W_1	BOX-W_2	–	–
	3.99	10.63	–	–

interaction. The computed IR spectrum of the optimized global minimum energy conformer reproduced the observed IR spectrum where the hydrogen bonded methanol chain was bound between N centre and C(2)–H of BIM molecule via O–H···N and $C(2)-H\cdots O_{CH_3OH}$ H-bonding interactions, respectively. LIF spectrum and 2c-R2PI spectra identified MBIM–methanol complexes with up to three methanol molecules. Except 1:1 complex, IR spectra of other two complexes showed enhancement in IR intensity for C(2)–H stretching transitions. Like in the MBIM–$W_{(2–4)}$ complexes, methanol molecules form H-bonded chain between N centre and C(2)–H of MBIM in MBIM–$M_{(2-3)}$ complexes. It was apparent from these studies that both water and methanol have very similar structural patterns in the complexes of BIM and MBIM.

In summary, the CH group in the BIM/MBIM/BOX is not sufficiently activated so as to compete with the conventional H-bonding donor/acceptor sites. However, ample evidence was provided that underscores the secondary role played by the C–H···O H-bonding interaction in facilitating the hydration or solvation shell of the substrate. Further, it also supports the role played by the C–H···O H-bond in anchoring the imidazole side chain in certain enzymatic reactions. The BEs of all the complexes are tabulated in Table 5. It can be seen that with increase in number of solvent molecules, the BE increases non-linearly. The increased red shifts and broadening of the H-bonded O–H stretch transitions with increased number of solvent molecules suggest the presence of cooperativity in these complexes[93,95].

7 TCNB/TFB Complexes

This section presents the complexes of highly activated C–H group, such as 1,2,4,5-tetracyanobenzene (TCNB) (Fig. 1) and 1,2,4,5-tetrafluorobenzene (TFB). In both these molecules, four strong electron withdrawing groups make the two C–H groups at the para position with respect to each other very active or polar and therefore can participate in C–H···Y (Y = HB acceptor) H-bonding. Ghosh et al.[39] recently reported the complexes of water with TCNB. The TFB complexes were reported by Mikami et al.[36–38]. In case of TCNB, the adjacent –CN groups can also act as HB acceptors. Therefore, relative propensity of C–H···Y H-bonding in the presence of conventional HB site was monitored for this system.

The combination of LIF and FDIR spectra showed that TCNB–water complexes with up to three water molecules were observed. The BO transitions of TCNB–W_1, TCNB–W_2, and TCNB–W_3 complexes were red shifted by 12, 38, and 50 cm^{-1}, respectively, with respect to that of the TCNB monomer. Figure 9 shows the FDIR spectra of TCNB monomer as well as its water complexes. In case of TCNB monomer, FDIR spectrum shows a weak transition at 3062 cm^{-1} that was assigned as the antisymmetric C–H stretch of TCNB. FDIR spectrum of TCNB–W_1 showed a strong transition at 3054 cm^{-1} that was assigned as the C–H stretch transition of the complex. The C–H stretch transition was red shifted by 8 cm^{-1} compared to that in the TCNB monomer and IR intensity was also highly enhanced indicating that C–H of TCNB in TCNB–W_1 complex was involved in the H-bonding interaction. Geometry optimizations of TCNB–W_1 complex at the *cp*-ωB97X-D/6-311++G** level predicted

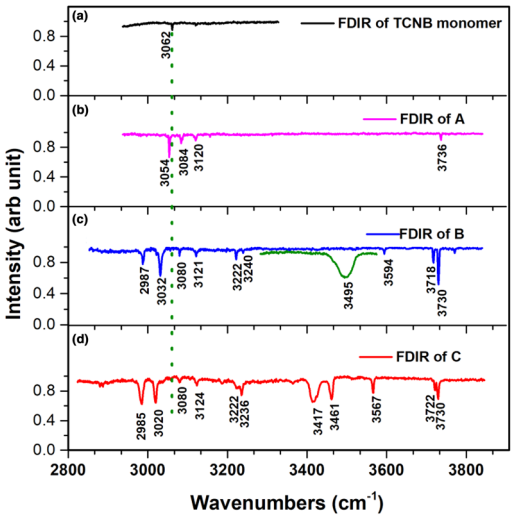

Figure 9: FDIR spectra of **a** TCNB monomer, **b** TCNB–W_1, **c** TCNB–W_2, and **d** TCNB–W_3. FDIR spectrum of TCNB–W_2 is an overlay of two traces, blue and green. Blue and green traces were recorded with $LiNbO_3$–OPO and KTP–OPO, respectively, as $LiNbO_3$–OPO does not have power in the green trace region. Green dotted line indicates the position of C–H stretch of TCNB monomer. Adapted with permission from Ref.[39]. Copyright © 2019 American Chemical Society.

four different conformers with the C–H···O HB bound conformer as the global minimum structure. The other conformers were OH···N bound and two π bound conformers. Based on the agreement between the experimental and computed IR spectra and the relative binding energies, it was suggested that the observed conformer was a C–H···O bound conformer, i.e. conformer 'a' as shown in Fig. 10. A point to be noted here is that the CH···O HB was the preferred mode of complex formation in preference to the conventional OH···N HB. Mikami et al.[36] have shown that in the 1:1 complex of 1,2,4,5-tetrafluorobenzene (TFB) with water, the C–H stretch frequency of TFB was also red shifted by 8 cm^{-1} and the IR intensity of the C–H stretch was significantly enhanced compared to that of TFB monomer. They concluded that one of the C–H group of TFB participated in H-bonding with water to form C–H···O H-bond to stabilize the complex. Similarly, C–H···O H-bond was also found in the complex of TFB with methanol where a red shift of 12 cm^{-1} was observed in the aromatic C–H stretch[37]. In all of the above cases, C–H···O H-bond played a primary role in the complex formation.

FDIR spectra of TCNB–$W_{2,3}$ showed intensity-enhanced transitions at 3032 and 3020 cm^{-1}, respectively, in the CH stretching region that were assigned as the C–H stretch transition in the respective complexes. The relative red shifts with respect to that in the monomer were 30 and 42 cm^{-1}, respectively. In addition, the FDIR spectrum of the TCNB–W_2 complex showed two red shifted O–H transitions at 3594 and 3495 cm^{-1} and two free O–H stretch transitions at 3730, 3718 cm^{-1}. With the help of computed IR spectra, the observed conformer to TCNB–W_2 complex was assigned to a conformer that has C–H···O bound hydrogen bonded water chain that bridges the C–H site with the N atom of adjacent –CN group as shown in Fig. 10. This result suggests that C–H moiety of TCNB plays a primary role in the building a water chain around the molecule, unlike the water complexes of BIM, MBIM, and BOX. The FDIR spectrum of TCNB–W_3 (Fig. 9d)

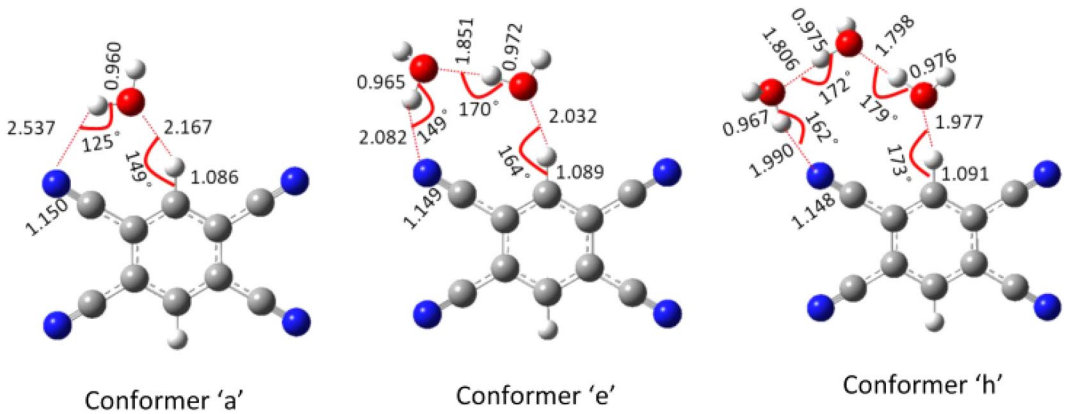

Figure 10: Observed conformers of TCNB–W_n (n= 1–3) calculated at *cp*-ωB97X-D/6-311++G** level of theory. H-bond-related geometrical parameters such as bond lengths in Å and bond angles are also mentioned. Reprinted with permission from Ref.[39]. Copyright © 2019 American Chemical Society.

showed five O–H stretch transitions with a few of them being greatly red shifted, besides the intensity-enhanced CH stretch at 3020 cm^{-1}. The number of other features that appear in the CH region of the FDIR spectra of TCNB–W_n ($n=2$, 3) were due to Fermi resonance of the CH bending overtones with the CH stretching mode of TCNB. With the help of BE calculation and computed IR spectra, it was confirmed that TCNB–W_3 also has the C–H···O bound H-bonded water bridge structure as shown in Fig. 10.

Above studies show that the first water molecule binds to the C–H site of TCNB/TFB in preference to the other sites. Addition of second water molecule in TCNB forms a hydrogen bonded water chain that bridges C–H site and –CN site via C–H···O HB and O–H···N HB, respectively. In case of TCNB–W_3 complex, the water molecules form an extended water chain. These results clearly suggest that C–H···O HB plays a primary role in developing hydration shell around TCNB. The H-bonded water/solvent chains bridging the HB donor and acceptor sites are common for conventional H-bonded systems[97]–[101] and are known to play s crucial role in proton shuttling across the chain[102]–[107]. H-bonded water chain growing on C–H site is very rare. We believe that H-bonded water chain at the activated C–H site can help in proton transfer from C–H site as well like conventional HB donor sites. Figure 10 also shows the geometrical parameters of TCNB–W_n ($n=1$–3) complexes. It can be seen that C–H···O H-bond length gradually decreases and ∠CHO becomes more linear (149°, 164°, 173°) in the TCNB–W_n complexes with increase in the number of water molecules. In other words, the C–H···O H-bond strength increases with increase in number of water molecules in the complex. Table 6 gives the computed binding energies of the observed conformers along with the AIM parameters. The increase in C–H···O H-bond strength is also reflected in the concomitant increase in the red shift in C–H stretch transition of TCNB that increases from 8 cm^{-1} in TCNB–W_1 complex to 42 cm^{-1} in TCNB–W_3 complex. Electron density at the BCP on C–H···O bond path and the second-order perturbation energy of the orbital overlap corresponding to lone pair of water oxygen and the antibonding orbital of C–H bond were also found to increase with the number of water molecules in the complex as shown in Table 6. AIM calculation suggested that significant changes in charge densities were found on the atoms which are involved in the hydrogen bonded cyclic ring structure of the TCNB–W_n complexes. This change in charge densities also brought cooperativity in the complexes. The cooperativity in case of TCNB–W_2 was found to be 2.43 kcal/mol and that of TCNB–W_3 was 5.21 kcal/mol. The increase in cooperativity with increase in number of water molecules in the complexes was also reflected in the H-bonded C–H and O–H stretching frequencies, as the red shifts of these transitions were found to increase with the number of water molecules.

8 Summary

The review summarizes the recent results on C–H···Y (Y = HB acceptor) H-bond in terms of spectroscopic characteristics and its role in molecular solvation that was carried out in our laboratory. Spectroscopic characterizations of red, blue, and zero shifted C–H···Y H-bonds were summarized for complexes of haloform with organic molecules such as 7-azaindole, 3-methylindole, *p*-cresol, and *p*-cyanophenol. The primary and secondary stabilization provided by C–H···Y H-bonds in molecular solvation for various organic molecules in water and alcohols were also discussed with the light of spectroscopy and ab initio/DFT calculations.

A summary of the electronic BO transitions of all the complexes and their corresponding C(2)–H stretch positions is tabulated in Table 7. The effect of para-substitution has nicely been brought out in the mode of interactions for the complexes of PCR and PCNP with haloforms. PCR forms C–H···π bound complexes with both $CHCl_3$ and CHF_3, whereas PCNP forms C–H···N bound complexes. In case of PCNP, the –CN group at the para position withdraws electron density from the π-electron cloud and destabilizes the C–H–π H-bond. In contrast, the π-electron density of the phenyl ring is enriched in PCR due to +I effect of the methyl group at the para position that enhances the stability of the C–H–π H-bond. Like most of the C–H–π bound complexes, PCR–haloform complexes also showed blue shifts in C–H stretch transition. In the C–H stretch frequency in PCNP–CHF_3 complex, however, a zero frequency shift was observed for PCNP–$CHCl_3$ complex. A considerably high blue shift of 27 cm^{-1} was observed for the C–H stretch frequency in PCNP–CHF_3 complex. Another important finding of these studies is that the normal mode frequencies are predicted well when calculations are performed using counterpoise corrected gradients. In the case of MI, C–H–π type complexes were observed with $CHCl_3$ and CHF_3. Even in the case of these heterocyclic polyaromatic molecules, the C–H–π

Table 6: Dissociation energies (D_0), electron density (ρ) at the H-bond critical points, and Laplacian of electron density ($\nabla^2\rho$) at the H-BCPs as shown in figure below. The numbers mentioned in the table refer to the BCPs shown in the figure. Corresponding second-order perturbation energies of overlapping orbitals (E^2) are also tabulated.

Complex[a]	D_0 (kcal/mol)	ρ at H-bond BCP (au)	$\nabla^2\rho$ at H-bond BCP (au)	E^2 (kcal/mol)
Conf 'a', $TCNB(H_2O)_1$	5.74[b] 4.65[c]	1) 0.0159, 2) 0.0077	1) -0.0148, 2) -0.0072	1) 4.36, 2) 0.06
Conf 'e', $TCNB(H_2O)_2$	13.42[b] 10.88[c]	1) 0.0211, 2) 0.0298, 3) 0.0182	1) -0.0199, 2) -0.0171, 3) -0.0271	1) 8.57, 2) 13.30, 3) 3.50
Conf 'h', $TCNB(H_2O)_3$	20.72[b]	1) 0.0235, 2) 0.0338, 3) 0.0331, 4) 0.0227	1) -0.0224, 2) -0.0299, 3) -0.0296, 4) -0.0208	1) 10.70, 2) 16.53, 3) 15.89, 4) 7.57

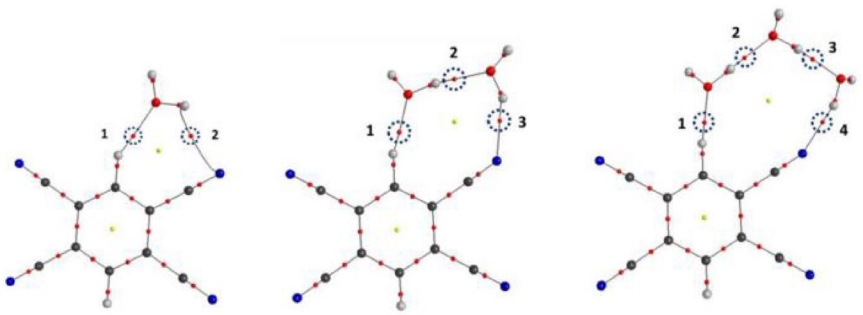

[a] Reference[39]
[b] Calculated at *cp*-ωB97X-D/6-311++G** level
[c] Calculated at *cp*-MP2/6-311++G** level

bound complexes showed a blue shift in the C–H stretch transition. In all the cases, the blue shift in the C–H stretching frequency was always higher for CHF_3 relative to that for $CHCl_3$ complexes.

The complexes of 7-azaindole with haloforms ($CHCl_3$, CHF_3) were exceptions. These complexes were found to be stabilized by coplanar C–H···N H-bonds. The C–H stretch frequency was greatly red shifted by 82 cm^{-1} compared to that in $CHCl_3$ monomer. Computationally even the CHF_3 complex was predicted to be red shifted, however, a blue shift 4 cm^{-1} in C–H stretch frequency was observed for AI–CHF_3 complex. The discrepancy in experimental and computational observations was reconciled by invoking Fermi mixing of the C–H stretch transition with the overtones of the C–H bend transition that caused shift in vibrational levels. This is an example of pseudo-blue shifted H-bonded complex. This C–H···N bound complex can be contrasted with the zero frequency shifted complex observed in the case of PCNP–$CHCl_3$ complex. It is conjectured that the hybridization of the nonbonding orbital on the N centre controls the interaction of the lone pair orbital with the antibonding orbital of the C–H bond that determines the red shift in the H-bond donor stretching frequency. It may be interesting to investigate the haloform complexes of another heterocyclic compounds, for example, benzimidazole that has the N centre as an acceptor.

Role of C–H···Y H-bond in the microsolvation of few organic molecules has been explored. It was found that in the 1:1 complexes of BIM, MBIM, and BOX with water and alcohols, the solvent molecules do not bind to the C(2)–H site of imidazole or oxazole moiety. However, the 1:2 complexes of these molecules showed formation of water bridge structure between N site of the imidazole/oxazole moiety and the C(2)–H site via O–H···N and $C(2)-H\cdots O_{H_2O}$ H-bonds, respectively. In BIM–W_{3-4} complexes, water molecules form water bridge between the N centre and the N–H site of imidazole moiety and it was apparent that the $C(2)-H\cdots O_{H_2O}$ H-bond

Table 7: Summary of electronic transitions and C(2)–H stretch transitions.

Complex	S_1–S_0 band origin shift (cm^{-1})	Shift in C–H stretch (cm^{-1})	D_0 in kcal/mol	Type of interaction
PCR–$CHCl_3$	+45	+11	6.80[a]	C–H···π
PCR–CHF_3	+101	+17	3.50[b]	
MI–$CHCl_3$	−22	+2	5.91[c]	
MI–CHF_3	+7	+16	4.17[c]	
PCNP–$CHCl_3$	+112	0	5.40[a]	CH···N
PCNP–CHF_3	+110	+27	3.70[a]	
AI–$CHCl_3$	−309	−82	6.46[a]	
AI–CHF_3	−243	+4	5.06[a]	
BIM complexes				
BIM–W_1 (A′)	–68	0	5.04[a]	N–H···O
BIM–W_1 (A)	+104	0	5.08[a]	O–H···N
BIM–W_1 (B)	+149	0	5.02[a]	O–H···N
BIM–W_2 (C)	+217	+14	12.02[a]	Multiple
BIM–W_3 (D)	+174	–	19.93[a]	Multiple
BIM–W_4 (E)	+185	–	28.07[a]	Multiple
BIM–M_1 (A′)	−103	–	6.11[b]	N–H···O
BIM–M_1 (A)	+108	–	5.87[b]	O–H···N
BIM–M_2 (B)	+223	+1	14.48[b]	Multiple
MBIM complexes				
MBIM–W_1 (A)	+117	0	5.28[a]	O–H···N
MBIM–W_1 (B)	+193	0	5.25[a]	O–H···N
MBIM–W_2 (C)	+286	−3	12.38[a]	Multiple
MBIM–W_3 (D)	+310	–	19.40[a]	Multiple
MBIM–W_4 (E)	+298	+14	25.04[a]	Multiple
MBIM–M_1	+130		6.14[b]	O–H···N
MBIM–M_2	+294	−12	14.85[b]	Multiple
MBIM–M_3	+313	+18	23.30[b]	Multiple
BOX complexes				
BOX–W_1 (A)	−27	–	4.37[a]	O–H···N
BOX–W_1 (B)	91	–	3.99[a]	O–H···N
BOX–W_2 (C)	149	–	10.63[a]	Multiple
TCNB complexes				
TCNB–W_1	−12	−8	5.74[d]	CH···O
TCNB–W_2	−38	−30	13.42[d]	
TCNB–W_3	−50	−42	20.72[d]	

[a] Calculated at *cp*-MP2/aug-cc-pVDZ level
[b] Calculated at MP2/aug-cc-pVDZ level
[c] Calculated at MP2/6-311++G** level
[d] Calculated at *cp*-ωB97X-D/6-311++G** level

was not able to compete with the conventional H-bond donor. However, in MBIM where the N–H was methylated, the water chain was held by the N centre and the C(2)–H site of imidazole via O–H···N and $C(2)-H\cdots O_{H_2O}$ H-bonds, respectively. The binding energies of MBIM–$W_{3–4}$ complexes were also found to be comparable to the BIM–$W_{3–4}$ complexes, i.e. stabilization provided

by $C(2)-H\cdots O_{H_2O}$ H-bond in MBIM–W_{3-4} complexes is comparable to the $N-H\cdots O_{H_2O}$ H-bonds in BIM–W_{3-4} complexes. Similarly, it was also observed that in the MBIM–M_{2-3} complexes the methanol molecules form a hydrogen bonded methanol bridge between the N centre and the C(2)–H site of MBIM. These studies conclusively suggest that C(2)–H···O H-bond plays an active role in molecular solvation by providing secondary stabilization to the H-bonded water network. In these complexes, the shift of C(2)–H stretch transitions was found to be mostly blue shifted except in the case of MBIM–W_2 or MBIM–M_2 complexes, but in all the IR intensity enhancement is noticeable. The shifts were also below 20 cm^{-1}.

In TCNB complexes with water, the C–H···O H-bonds were found to play a primary role in the molecular solvation of TCNB–W_n ($n=1$–3) complexes. It has been found that first water molecule binds to the C–H site of TCNB instead of N atoms of CN groups. Subsequent addition of water molecules forms a H-bonded water chain between C–H site and N atom of CN group forming ring structures. Enhancement of IR transition intensity and red shift in C–H stretch transition in these complexes are indicative of C–H···O H-bond formations in these complexes. The CH group was sufficiently activated in this molecule that in some sense it almost behaved like a conventional H-bond donor. A significant extent of cooperative effect was observed in all the H-bonded bridge structures in the TCNB complexes as well as BMI/MBIM/BOX complexes.

Publisher's Note

Springer Nature remains neutral with regard to jurisdictional claims in published maps and institutional affiliations.

Acknowledgements

SJW would like to acknowledge the exemplary hard work and dedication shown by his students Drs. Pranav Shirhatti, Aditi Bhattacherjee, and Sanat Ghosh whose work is presented in the review. The technical support provided by Mr Ajay Patil and Mr Sachin Temkar is also gratefully acknowledged. The work was supported by the Tata Institute of Fundamental Research, Mumbai via project no. 12-R&D-TFR-5.10-0100.

Received: 14 October 2019 Accepted: 2 December 2019
Published online: 21 December 2019

References

1. Desiraju GR, Steiner T (1999) The weak hydrogen bond in structural chemistry and biology. Oxford University Press, New York, pp 29–121
2. Moore TS, Winmill TF (1912) The state of amines an aqueous solution. J Chem Soc 101:1635–1676
3. Latimer WM, Rodebush WH (1920) Polarity and ionization from the standpoint of the Lewis theory of valence. J Am Chem Soc 42:1419–1433
4. Biswal HS, Chakraborty S, Wategaonkar S (2008) Experimental evidence of OH···S hydrogen bonding in supersonic jet. J Chem Phys 129:184311–184317
5. Mundlapati VR, Sahoo DK, Ghosh S, Purame UK, Pandey S, Acharya R, Pal N, Tiwari P, Biswal HS (2017) Spectroscopic evidences for strong hydrogen bonds with selenomethionine in proteins. J Phys Chem Lett 8:794–800
6. Sobczyk L, Grabowski SJ, Krygowski TM (2005) Interrelation between H-bond and Pi-electron delocalization. Chem Rev 105:3513–3560
7. Sutor DJ (1962) C–H···O hydrogen bond in crystals. Nature 195:68–69
8. Sutor DJ (1963) Evidence for existence of C–H···O hydrogen bonds in crystals. J Chem Soc 1105-1110
9. Taylor R, Kennard O (1982) Crystallographic evidence for the existence of C–H···O, C–H···N, and C–H···C1 hydrogen-bonds. J Am Chem Soc 104:5063–5070
10. Wahl MC, Sundaralingam M (1997) C–H···O hydrogen bonding in biology. Trends Biochem Sci 22:97–102
11. Senes A, Ubarretxena-Belandia I, Engelman DM (2001) The C–H···O hydrogen bond: a determinant of stability and specificity in transmembrane helix interactions. Proc Natl Acad Sci USA 98:9056–9061
12. Horowitz S, Trievel RC (2012) Carbon-oxygen hydrogen bonding in biological structure and function. J Biol Chem 287:41576–41582
13. Brovarets OO, Yurenko YP, Hovorun DM (2014) Intermolecular CH···O/N H-bonds in the biologically important pairs of natural nucleobases: a thorough quantum-chemical study. J Biomol Struct Dyn 32:993–1022
14. Yurenko YP, Zhurakivsky RO, Samijlenko SP, Hovorun DM (2011) Intramolecular CH···O hydrogen bonds in the AI and BI DNA-like conformers of canonical nucleosides and their Watson-Crick Pairs, quantum chemical and AIM analysis. J Biomol Struct Dyn 29:51–65
15. Jiang L, Lai LH (2002) CH···O hydrogen bonds at protein–protein interfaces. J Biol Chem 277:37732–37740
16. Thakur TS, Kirchner MT, Blaser D, Boese R, Desiraju GR (2010) C–H···F–C hydrogen bonding in 1,2,3,5-tetrafluorobenzene and other fluoroaromatic compounds and the crystal structure of alloxan revisited. CrystEngComm 12:2079–2085
17. Chatterjee J, Mierke DF, Kessler H (2008) Conformational preference and potential templates of

N-methylated cyclic pentaalanine peptides. Chem Eur J 14:1508–1517

18. Erez E, Fass D, Bibi E (2009) How intramembrane proteases bury hydrolytic reactions in the membrane. Nature 459:371–378
19. Desiraju GR (1991) The CH···O hydrogen bond in crystals: what is it? Acc Chem Res 24:290–296
20. Gu Y, Kar T, Scheiner S (1999) Fundamental properties of the CH···O interaction: is it a true hydrogen bond? J Am Chem Soc 121:9411–9422
21. Scheiner S, Kar T, Gu Y (2001) Strength of the Cα-H···O hydrogen bond of amino acid residues. J Biol Chem 276:9832–9837
22. Steiner T, Saenger W (1993) Role of CH···O hydrogen bonds in the coordination of water molecules. Analysis of neutron diffraction data. J Am Chem Soc 115:4540–4547
23. Kar T, Scheiner S (2004) Comparison of cooperativity in CH···O and OH···O hydrogen bonds. J Phys Chem A 108:9161–9168
24. Popelier P, Bader R (1992) The existence of an intramolecular C–H···O hydrogen bond in creatine and carbamoyl sarcosine. Chem Phys Lett 189:542–548
25. Pierce AC, Sandretto KL, Bemis GW (2002) Kinase inhibitors and the case for CH···O hydrogen bonds in protein–ligand binding. Proteins Struct Funct Bioinform 49:567–576
26. Braga D, Grepioni F, Biradha K, Pedireddi V, Desiraju GR (1995) Hydrogen bonding in organometallic crystals. 2. CH···O hydrogen bonds in bridged and terminal first-row metal carbonyls. J Am Chem Soc 117:3156–3166
27. Samanta AK, Chakraborty T (2010) In: Chaudhuri RK, Mekkaden MV, Raveendran AV, Satya Narayanan A (eds) Recent advances in spectroscopy. Springer, pp 53–61
28. Mukhopadhyay A, Mukherjee M, Pandey P, Samanta AK, Bandyopadhyay B, Chakraborty T (2009) Blue shifting C−H···O hydrogen bonded complexes between chloroform and small cyclic ketones: ring-size effects on stability and spectral shifts. J Phys Chem A 113:3078–3087
29. Reimann B, Buchhold K, Vaupel S, Brutschy B, Havlas Z, Spirko V, Hobza P (2001) Improper, blue-shifting hydrogen bond between fluorobenzene and fluoroform. J Phys Chem A 105:5560–5566
30. Shirhatti PR, Maity DK, Wategaonkar S (2013) C-H···Y hydrogen bonds in the complexes of *p*-cresol and *p*-cyanophenol with fluoroform and chloroform. J Phys Chem A 117:2307–2316
31. Shirhatti PR, Wategaonkar S (2010) Blue shifted hydrogen bond in 3-methylindole·CHX_3 complexes (X = Cl, F). Phys Chem Chem Phys 12:6650–6659
32. Delanoye SN, Herrebout WA, van der Veken BJ (2002) Improper or classical hydrogen bonding? A comparative cryosolutions infrared study of the complexes of $HCClF_2$, $HCCl_2F$, and $HCCl_3$ with dimethyl ether. J Am Chem Soc 124:7490–7498
33. Delanoye SN, Herrebout WA, van der Veken BJ (2002) Blue shifting hydrogen bonding in the complexes of chlorofluoro haloforms with acetone-d_6 and oxirane-d_4. J Am Chem Soc 124:11854–11855
34. Michielsen B, Dom JJJ, van der Veken BJ, Hesse S, Xue ZF, Suhm MA, Herrebout WA (2010) The complexes of halothane with benzene: the temperature dependent direction of the complexation shift of the aliphatic C–H stretching. Phys Chem Chem Phys 12:14034–14044
35. van der Veken BJ, Herrebout WA, Szostak R, Shchepkin DN, Havlas Z, Hobza P (2001) The nature of improper, blue-shifting hydrogen bonding verified experimentally. J Am Chem Soc 123:12290–12293
36. Venkatesan V, Fujii A, Ebata T, Mikami N (2004) A direct experimental evidence for an aromatic C–H···O hydrogen bond by fluorescence-detected infrared spectroscopy. Chem Phys Lett 394:45–48
37. Venkatesan V, Fujii A, Ebata T, Mikami N (2005) Infrared and ab initio studies on 1,2,4,5-tetrafluorobenzene clusters with methanol and 2,2,2-trifluoroethanol: presence and absence of an aromatic C–H···O hydrogen bond. J Phys Chem A 109:915–921
38. Venkatesan V, Fujii A, Mikami N (2005) A study on aromatic C–H···X (X = N, O) hydrogen bonds in 1,2,4,5-tetrafluorobenzene clusters using infrared spectroscopy and ab initio calculations. Chem Phys Lett 409:57–62
39. Ghosh S, Wategaonkar S (2019) C–H···O hydrogen bond anchored water bridge in 1,2,4,5-tetracyanobenzene-water clusters. J Phys Chem A 123:3851–3862
40. Samanta AK, Banerjee P, Bandyopadhyay B, Pandey P, Chakraborty T (2017) Antagonistic interplay between an intermolecular CH···O and an intramolecular OH···O hydrogen bond in a 1: 1 complex between 1, 2-cyclohexanedione and chloroform: a combined matrix isolation infrared and quantum chemistry study. J Phys Chem A 121:6012–6020
41. Sundararajan K, Ramanathan N (2007) Infrared and ab initio study of acetylene–acetone complex in solid argon and nitrogen matrices. J Mol Struct 833:150–160
42. Jemmis E, Giju K, Sundararajan K, Sankaran K, Vidya V, Viswanathan K, Leszczynski J (1999) An ab initio and matrix isolation infrared study of the 1:1 C_2H_2–$CHCl_3$ adduct. J Mol Struct 510:59–68
43. Gopi R, Ramanathan N, Sundararajan K (2014) Experimental evidence for blue-shifted hydrogen bonding in the fluoroform–hydrogen chloride complex: a matrix-isolation infrared and ab initio study. J Phys Chem A 118:5529–5539
44. Gopi R, Ramanathan N, Sundararajan K (2015) Hydrogen-bonded complexes of acetylene and acetonitrile: a matrix isolation infrared and computational study. J Mol Struct 1083:364–373

45. Sarkar S, Ramanathan N, Gopi R, Sundararajan K (2017) Pyrrole multimers and pyrrole-acetylene hydrogen bonded complexes studied in N_2 and *para*-H_2 matrixes using matrix isolation infrared spectroscopy and ab initio computations. J Mol Struct 1149:387–403
46. Gopi R, Ramanathan N, Sundararajan K (2017) Experimental evidence for the blue-shifted hydrogen-bonded complexes of CHF_3 with π-electron donors. Spectrochim Acta Part A Mol Biomol Spectrosc 181:137–147
47. Hobza P, Spirko V, Selzle HL, Schlag EW (1998) Anti-hydrogen bond in the benzene dimer and other carbon proton donor complexes. J Phys Chem A 102:2501–2504
48. Hobza P, Spirko V, Havlas Z, Buchhold K, Reimann B, Barth HD, Brutschy B (1999) Anti-hydrogen bond between chloroform and fluorobenzene. Chem Phys Lett 299:180–186
49. Yamamoto R, Ebata T, Mikami N (2001) Mode dependent intracluster vibrational energy redistribution rate in size-selected benzonitrile-$(CHCl_3)_{n=1-3}$ clusters. J Chem Phys 114:7866–7876
50. Hobza P, Havlas Z (2000) Blue-shifting hydrogen bonds. Chem Rev 100:4253–4264
51. Hobza P, Havlas Z (2002) Improper, blue-shifting hydrogen bond. Theor Chem Acc 108:325–334
52. Hobza P (2001) The H-index unambiguously discriminates between hydrogen bonding and improper blue-shifting hydrogen bonding. Phys Chem Chem Phys 3:2555–2556
53. Hermansson K (2002) Blue-shifting hydrogen bonds. J Phys Chem A 106:4695–4702
54. Pejov L, Hermansson K (2003) On the nature of blue shifting hydrogen bonds: ab initio and density functional studies of several fluoroform complexes. J Chem Phys 119:313–324
55. Alabugin IV, Manoharan M, Peabody S, Weinhold F (2003) Electronic basis of improper hydrogen bonding: a subtle balance of hyperconjugation and rehybridization. J Am Chem Soc 125:5973–5987
56. Joseph J, Jemmis ED (2007) Red-, blue-, or no-shift in hydrogen bonds: a unified explanation. J Am Chem Soc 129:4620–4632
57. Levy DH (1980) Laser Spectroscopy of cold gas-phase molecules. Annu Rev Phys Chem 31:197–225
58. Levy DH (1981) The spectroscopy of very cold gases. Science 214:263–269
59. Zare RN (2012) My life with LIF: a personal account of developing laser-induced fluorescence. Annu Rev Anal Chem 5:1–14
60. Friedrich DM, Mcclain WM (1980) 2-photon molecular electronic spectroscopy. Annu Rev Phys Chem 31:559–577
61. Ashfold MNR, Howe JD (1994) Multiphoton spectroscopy of molecular-species. Annu Rev Phys Chem 45:57–82
62. Brutschy B (2000) The structure of microsolvated benzene derivatives and the role of aromatic substituents. Chem Rev 100:3891–3920
63. Wiley WC, McLaren IH (1955) Time-of-flight mass spectrometer with improved resolution. Rev Sci Instrum 26:1150–1157
64. Rothman LS, Jacquemart D, Barbe A, Benner DC, Birk M, Brown L, Carleer M, Chackerian C Jr, Chance K, Coudert L et al (2005) The HITRAN 2004 molecular spectroscopic database. J Quant Spectrosc Radiat Transf 96:139–204
65. Frisch MJ, Trucks GW, Schlegel HB, Scuseria GE, Robb MA, Cheeseman JR, Scalmani G, Barone V, Mennucci B, Petersson GA, Nakatsuji H, Caricato M, Li X, Hratchian HP, Izmaylov AF, Bloino J, Zheng G, Sonnenberg JL, Hada M, Ehara M, Toyota K, Fukuda R, Hasegawa J, Ishida M, Nakajima T, Honda Y, Kitao O, Nakai H, Vreven T, Montgomery JA Jr., Peralta JE, Ogliaro F, Bearpark M, Heyd JJ, Brothers E, Kudin KN, Staroverov VN, Keith T, Kobayashi R, Normand J, Raghavachari K, Rendell A, Burant JC, Iyengar SS, Tomasi J, Cossi M, Rega N, Millam JM, Klene M, Knox JE, Cross JB, Bakken V, Adamo C, Jaramillo J, Gomperts R, Stratmann RE, Yazyev O, Austin AJ, Cammi R, Pomelli C, Ochterski JW, Martin RL, Morokuma K, Zakrzewski VG, Voth GA, Salvador P, Dannenberg JJ, Dapprich S, Daniels AD, Farkas O, Foresman JB, Ortiz JV, Cioslowski J, Fox DJ (2010) Gaussian 09, Revision C.01, Gaussian, Inc. Wallingford CT
66. Bader RFW (1991) A quantum theory of molecular structure and its applications. Chem Rev 91:893–928
67. Koch U, Popelier PLA (1995) Characterization of C–H···O hydrogen bonds on the basis of the charge density. J Phys Chem 99:9747–9754
68. Glendening ED, Landis CR, Weinhold F (2013) NBO 6.0: natural bond orbital analysis program. J Comput Chem 34:1429–1437
69. Reed AE, Curtiss LA, Weinhold F (1988) Intermolecular interactions from a natural bond orbital, donor-acceptor viewpoint. Chem Rev 88:899–926
70. Schmidt MW, Baldridge KK, Boatz JA, Elbert ST, Gordon MS, Jensen JH, Koseki S, Matsunaga N, Nguyen KA, Su SJ, Windus TL, Dupuis M, Montgomery JA (1993) General atomic and molecular electronic-structure system. J Comput Chem 14:1347–1363
71. Morita S, Fujii A, Mikami N, Tsuzuki S (2006) Origin of the attraction in aliphatic C–H/π interactions: infrared spectroscopic and theoretical characterization of gas-phase clusters of aromatics with methane. J Phys Chem A 110:10583–10590
72. Biswal HS, Wategaonkar S (2009) Sulfur, not too far behind O, N, and C: SH···π hydrogen bond. J Phys Chem A 113:12774–12782
73. Tsuzuki S, Honda K, Uchimaru T, Mikami M, Tanabe K (2002) The interaction of benzene with chloro- and

fluoromethanes: effects of halogenation on CH/π interaction. J Phys Chem A 106:4423–4428
74. Li X, Liu L, Schlegel HB (2002) On the physical origin of blue-shifted hydrogen bonds. J Am Chem Soc 124:9639–9647
75. Shirhatti PR, Maity DK, Bhattacharyya S, Wategaonkar S (2014) C–H···N hydrogen-bonding interaction in 7-Azaindole:CHX_3 (X = F, Cl) complexes. ChemPhysChem 15:109–117
76. Qian WL, Krimm S (2002) Vibrational spectroscopy of hydrogen bonding: origin of the different behavior of the C–H···O hydrogen bond. J Phys Chem A 106:6628–6636
77. Krajewska M, Olbert-Majkut A, Mielke Z (2002) Matrix infrared spectra and ab initio calculations of the acetylene complexes with nitric and nitrous acids. Phys Chem Chem Phys 4:4305–4313
78. Tatamitani Y, Liu BX, Shimada J, Ogata T, Ottaviani P, Maris A, Caminati W, Alonso JL (2002) Weak, improper, C-O···H-C hydrogen bonds in the dimethyl ether dimer. J Am Chem Soc 124:2739–2743
79. Lockwood SP, Fuller TG, Newby JJ (2018) Structure and spectroscopy of Furan:H_2O complexes. J Phys Chem A 122:7160–7170
80. Hussein MA, Millen DJ (1976) Hydrogen-bonding in gas-phase. 4. Infrared spectroscopic investigation of O-H···O and C–H···N complexes–alcohol + ether and trichloromethane + amine systems. J Chem Soc Farad Trans II 72:693–699
81. Rutkowski KS, Karpfen A, Melikova SM, Herrebout WA, Koll A, Wolschann P, van der Veken BJ (2009) Cryospectroscopic and ab initio studies of haloform-trimethylamine H-bonded complexes. Phys Chem Chem Phys 11:1551–1563
82. Herrebout WA, Melikova SM, Delanoye SN, Rutkowski KS, Shchepkin DN, van der Veken BJ (2005) A cryosolution infrared study of the complexes of fluoroform with ammonia and pyridine: evidence for a C–H···N pseudo blue-shifting hydrogen bond. J Phys Chem A 109:3038–3044
83. Guin M, Patwari GN, Karthikeyan S, Kim KS (2011) Do N-heterocyclic aromatic rings prefer π-stacking? Phys Chem Chem Phys 13:5514–5525
84. Hippler M (2007) Quantum chemical study and infrared spectroscopy of hydrogen-bonded $CHCl_3$–NH_3 in the gas phase. J Chem Phys 127:084306
85. Hippler M, Hesse S, Suhm MA (2010) Quantum-chemical study and FTIR jet spectroscopy of $CHCl_3$–NH_3 association in the gas phase. Phys Chem Chem Phys 12:13555–13565
86. Paulson SL, Barnes AJ (1982) Trihalogenomethane—base complexes studied by vibrational spectroscopy in low-temperature matrices. J Mol Struct 80:151–158
87. Gord JR, Garrett AW, Bandy RE, Zwier TS (1990) Rempi fragmentation as a probe of hydrogen-bonding in aromatic-X clusters. Chem Phys Lett 171:443–450
88. Fujii A, Shibasaki K, Kazama T, Itaya R, Mikami N, Tsuzuki S (2008) Experimental and theoretical determination of the accurate interaction energies in benzene–halomethane: the unique nature of the activated CH/π interaction of haloalkanes. Phys Chem Chem Phys 10:2836–2843
89. Jin Z (2006) Imidazole, oxazole and thiazole alkaloids. Nat Prod Rep 23:464–496
90. Ghosh S, Reddy CM (2012) Elastic and bendable caffeine cocrystals: implications for the design of flexible organic materials. Angew Chem Int Ed 51:10319–10323
91. Garist IV, Verevkin SP, Bara JE, Hindman MS, Danielsen SP (2012) Building blocks for ionic liquids: vapor pressures and vaporization enthalpies of 1-(*n*-alkyl)-benzimidazoles. J Chem Eng Data 57:1803–1809
92. Bhattacherjee A, Wategaonkar S (2015) Conformational preferences of monohydrated clusters of imidazole derivatives revisited. Phys Chem Chem Phys 17:20080–20092
93. Bhattacherjee A, Wategaonkar S (2017) Role of the C(2)–H hydrogen bond donor in gas-phase microsolvation of imidazole derivatives with ROH (R = CH_3, C_2H_5). J Phys Chem A 121:4283–4295
94. Bhattacherjee A, Wategaonkar S (2017) Conformational heterogeneity and the role of the C(2)–H donor in mono- and dihydrated clusters of benzoxazole. J Phys Chem A 121:5420–5427
95. Bhattacherjee A, Wategaonkar S (2016) Water bridges anchored by a C–H···O hydrogen bond: the role of weak interactions in molecular solvation. Phys Chem Chem Phys 18:27745–27749
96. Talbot F, Simons J (2002) Infrared ion dip and ultraviolet spectroscopy of 4-phenyl imidazole, its tautomer, 5-phenyl imidazole, and its multiply hydrated clusters. Eur Phys J D At Mol Opt Plasma Phys 20:389–398
97. Coussan S, Manca C, Tanner C, Bach A, Leutwyler S (2003) Ammonia-chain clusters: vibronic spectra of 7-hydroxyquinoline·$(NH_3)_2$. J Chem Phys 119:3774–3784
98. Matsumoto Y, Ebata T, Mikami N (2001) OH stretching vibrations and hydrogen-bonded structures of 7-hydroxyquinoline-$(H_2O)_{1-3}$ investigated by IR–UV double-resonance spectroscopy. Chem Phys Lett 338:52–60
99. Snoek LC, Kroemer RT, Simons JP (2002) A spectroscopic and computational exploration of tryptophan–water cluster structures in the gas phase. Phys Chem Chem Phys 4:2130–2139
100. Carney JR, Dian BC, Florio GM, Zwier TS (2001) The role of water bridges in directing the conformational preferences of 3-indole-propionic acid and tryptamine. J Am Chem Soc 123:5596–5597
101. Nakajima A, Hirano M, Hasumi R, Kaya K, Watanabe H, Carter C, Williamson J, Miller TA (1997) High-resolution laser-induced fluorescence spectra of 7-Azaindole–water complexes and 7-azaindole dimer. J Phys Chem A 101:392–398
102. Tanner C, Manca C, Leutwyler S (2003) Probing the threshold to H atom transfer along a hydrogen-bonded ammonia wire. Science 302:1736–1739

103. Garczarek F, Gerwert K (2006) Functional waters in intraprotein proton transfer monitored by FTIR difference spectroscopy. Nature 439:109–112
104. Freier E, Wolf S, Gerwert K (2011) Proton transfer via a transient linear water-molecule chain in a membrane protein. Proc Natl Acad Sci USA 108:11435–11439
105. Kaila VRI, Hummer G (2011) Energetics and dynamics of proton transfer reactions along short water wires. Phys Chem Chem Phys 13:13207–13215
106. Park SY, Kim B, Lee YS, Kwon OH, Jang DJ (2009) Triple proton transfer of excited 7-hydroxyquinoline along a hydrogen-bonded water chain in ethers: secondary solvent effect on the reaction rate. Photochem Photobiol Sci 8:1611–1617
107. Folmer DE, Wisniewski ES, Stairs JR, Castleman AW (2000) Water-assisted proton transfer in the monomer of 7-azaindole. J Phys Chem A 104:10545–10549

Sanjay Wategaonkar is a senior professor in the Department of Chemical Sciences at the Tata Institute of Fundamental Research, Mumbai. He has been working in the area of supersonic jet spectroscopy of small molecules and non-covalently bonded weak complexes, unravelling intra-molecular processes such as vibrational energy distribution and predissociation using laser spectroscopy. Recent focus of his research has been the investigation of the properties and strength of unconventional hydrogen bonded complexes.

Sanat Ghosh has done his M.Sc. from the University of Burdwan, West Bengal and Ph.D. from Tata Institute of Fundamental Research, Mumbai under the guidance of Sanjay Wategaonkar. He spent one and a half year in RIKEN, Wako, Japan before joining Luis Banares at Universidad Complutense de Madrid, Spain. He has mainly worked in the area of laser spectroscopy of hydrogen bonded complexes synthesized using supersonic jet expansion method. He is also experienced in the heterodyne detected vibrational sum frequency generation spectroscopy employed at the solid/liquid buried interfaces.